

An improved criterion to select dominant modes from dynamic mode decomposition

Jiaqing Kou, Weiwei Zhang*

School of Aeronautics, Northwestern Polytechnical University, Xi'an 710072, China



ARTICLE INFO

Article history:

Received 27 July 2016

Received in revised form

11 November 2016

Accepted 15 November 2016

Available online 7 December 2016

Keywords:

Dynamic mode decomposition

Reduced-order model

Unsteady flow

Transonic flow

Buffet

ABSTRACT

Dynamic mode decomposition (DMD) has been extensively utilized to analyze the coherent structures in many complex flows. Although specific flow patterns with dominant frequency and growth rate can be captured, extracting dominant DMD modes for flow reconstruction and dynamic modeling still needs a priori knowledge on flow physics, especially for some transient states of unstable flows. In this paper, a criterion to select dominant modes from DMD technique is developed. The unsteady flow can be described by the superposition of each normalized DMD mode multiplied by its time coefficient. The dominance of each DMD mode can be ordered by time integration of its time coefficient. Compared with standard DMD approach, which decides the dominance of DMD modes from the order of amplitude or mode norm, this criterion considers the evolution of each mode within the whole sampling space, and ranks them according to their contribution to all samples. The proposed mode selection strategy is evaluated by test cases including both equilibrium and transient states of a cylinder at Reynolds number of 60 and a transient state of a NACA0012 airfoil buffeting in transonic flow. Results indicate that using this criterion, dominant DMD modes can be identified and flow dynamics in unstable or transient systems can be reconstructed accurately with fewer modes. Besides, this approach has better convergence against mode number and lower sensitivity to the initial condition than standard DMD method.

© 2016 Elsevier Masson SAS. All rights reserved.

1. Introduction

Developing reduced-order models (ROMs) for complex fluid flows permits a wide range of engineering applications including mechanism analysis, dynamic modeling, control law design and optimization. Among current investigations in modeling dynamic systems for control and stability analysis, constructing ROM based on input–output data usually provides satisfactory results, which is called system identification. Autoregressive with exogenous input model [1] and neural networks [2–4] are typical identification-based ROMs that have been extensively used in unsteady aerodynamic modeling and aeroelasticity. However, when studying the dynamics of a full-order fluid flow, mode decomposition techniques are more appropriate to be utilized, which decompose the unsteady flow into several dominant coherent structures. Proper orthogonal decomposition (POD) [5, 6], dynamic mode decomposition (DMD) [7,8] and global stability analysis [9,10] have all been introduced to extract features on flow

dynamics and stabilities, and the selected dominant flow modes are important in constructing low-dimensional dynamic models for flow prediction and control. Based on spatial correlation of flow snapshots, POD decomposes the dataset into an orthogonal set of modes that contain multiple frequency components to represent dominant and coherent flow features, and ranks each mode by its energy content. Derived from linear tangent approximation or linear Koopman operator which is able to capture nonlinear dynamics as it describes the evolution of observables, another technique of flow feature extraction called DMD is developed. Given by a data-driven algorithm, DMD obtains non-orthogonal modes with a single frequency to capture important dynamic effects. Once the dominant flow modes are obtained, the evolution of unsteady flows can be described by the superposition of these dynamic structures and their time coefficients.

Modeling dynamic systems by mode decomposition techniques depends on two aspects, i.e., the selected modes and the temporal evolution of time coefficients. On the one hand, selecting dominant POD modes based on energy content is a reliable methodology, but ranking DMD modes is not unique, which is the focus of this study. On the other hand, although significant POD modes can be decided easily by energy order, extrapolation of time coefficients is not easy. There are two classes of ROM methods to

* Corresponding author.

E-mail addresses: koujiaqing93@163.com (J. Kou), [\(W. Zhang\).](mailto:aeroelastic@nwpu.edu.cn)

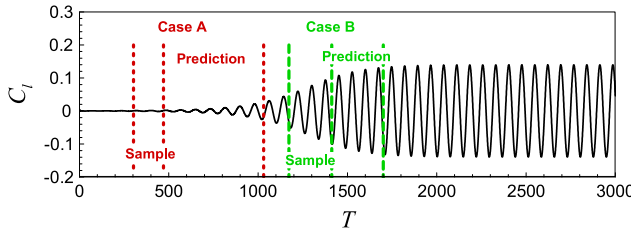


Fig. 1. Temporal evolution of lift coefficient at $Re = 60$.

identify the development of POD time coefficients: nonintrusive and intrusive modeling [11,12]. Intrusive methods project the orthogonal modes onto the original system of partial differential equations and build a system described by ordinary differential equations [5,13,14], whereas nonintrusive methods utilize some surrogate models for coefficient interpolation [11,12,15]. But DMD technique is more convenient in modeling flow dynamics since all the available dynamic modes are accompanied by the temporal dynamics characterized by the corresponding mode eigenvalues. This advantage makes the data-driven DMD approach an effective methodology for modeling complex turbulent flows.

Since its appearance, DMD has attracted many researchers for its relative simplicity [16–18]. Thereafter, a number of studies have been conducted in order to improve the pre-processing or the post-processing capability of standard DMD. These strategies range from ensemble-averaging method [19] and sparsity promoting approaches [20,21] to improved least-squares methods [22–25]. DMD approach is also linked with nonlinear system description using machine-learning approaches by Nathan Kutz et al. [26–29]. Moreover, a better understanding of DMD algorithm is obtained through analyzing the effects of noise [30] and considering data update [31], sub-Nyquist-rate data [32], or arbitrarily sampled systems [33]. To allow control law design, DMD with control [34] and input–output DMD [35] have been developed. Furthermore, it is worth noting that an interesting recent development is recursive DMD [36], which combines POD and DMD to obtain orthonormal DMD modes that have a natural ordering. This study has interpreted a complete transient process from the steady solution to the post-transient attractor through a modal perspective. Applications of DMD method on fluid problems include boundary layer flows [37], transitional jets [38], transition of an airfoil [39] and backward-facing step flow [40], which are well documented in [41].

With these recent studies, standard DMD method addresses the problems in optimal mode decomposition and data sampling. However, the criterion to extract dominant DMD modes for ROM construction is not unique, which is the focus of current study. The aim of mode selection is to find a compact representation of unsteady flows by a small number of DMD modes and provide the optimal approximation of physical features on the sampled or predicted flow. Rowley et al. [7] and Wan et al. [38] ranked the Koopman modes by ordering the norm of each mode. This method

Table 1

Dominant DMD modes of the equilibrium state from DMD and DMD with criterion approaches.

DMD			DMD with criterion		
Mode	Growth rate	St	Mode	Growth rate	St
1	0	0	1	0	0
2	4.7994×10^{-3}	0.1207	2	4.7994×10^{-3}	0.1207
3	-5.2243×10^{-3}	0.1049	3	8.7328×10^{-3}	0
4	8.7328×10^{-3}	0	4	-5.2243×10^{-3}	0.1049
5	-3.1934×10^{-2}	0.1372	5	9.6633×10^{-3}	0.2412

may not be effective when some modes with a large norm and a large damp exist. Schmid et al. [42] defined the mode amplitude computed by projecting the data sequence onto the identified dynamic modes, and the coefficients of this projection indicate the significance of specific dynamic modes. This method may ignore the influence of each mode's stability characteristics. In addition, projecting the modes on the first snapshot of the data is also preferred, as shown by Sayadi et al. [43]. This approach can be suboptimal if the selected modes have a large decay-rate. Jovanović et al. [20] defined the amplitude based on the modal contribution of the reduced first snapshot and optimized the amplitudes over the whole dataset. However, since in the first step, the amplitudes are not optimized, some numerically transient modes with large amplitudes may also be included in the sparsity structure. The problem of existing transient modes is also noticed by Tu et al. [44], where the norm of the modes is weighted by the magnitude of the corresponding DMD eigenvalues to penalize spurious modes with large norms but large decay rates. This criterion will reflect the contribution of each mode more accurately than the criterion based merely on mode norms. Furthermore, a criterion based on the time-averaged modal energy contribution was introduced in [45], which is similar to current scaling definition. Recently, Sayadi et al. [21] proposed a parametrized DMD approach, which firstly determined a sparsity structure and then redefined the amplitude of each DMD mode as a time-dependent coefficient and integrated the amplitudes in time to achieve data extrapolation. Compared with standard DMD with fixed amplitudes in time, this approach is able to identify the dominant modes of thermo-acoustically unstable systems.

It should be noted that all the mode selection strategies mentioned above are effective in capturing dominant flow modes of periodic flows or complete linear systems [7]. This is because in most of periodic or linear flows, the magnitude of each mode differs significantly, and the dominant modes can be easily identified from the initial condition or each mode norm. However, for unstable systems (e.g., the transient state of a cylinder at low Reynolds number or a transonic flow with a moving shock wave) or highly turbulent flows, capturing the dominant flow features becomes hard, since multiple basic frequencies may exist and more numerically transient modes are needed to fully approximate the samples. To accurately order the importance of each mode, both the initial condition and the mode development within the whole

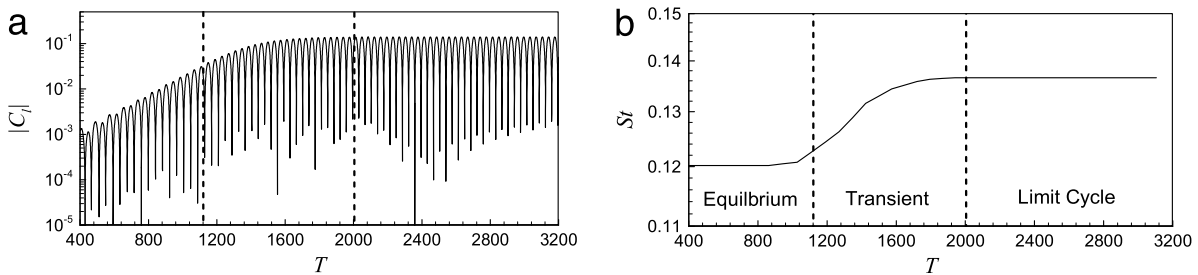


Fig. 2. Amplitude and frequency characteristics of lift coefficient at $Re = 60$. (a) Abstract value of lift coefficient changes with time (b) The corresponding instantaneous Strouhal number.

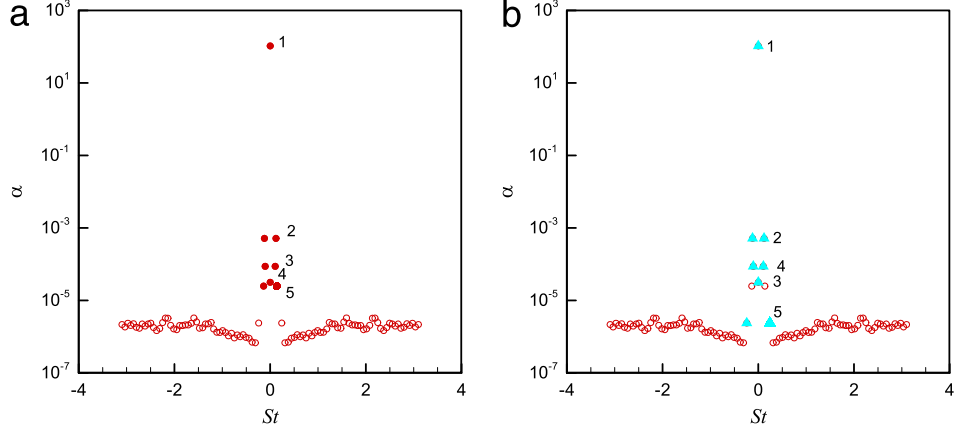


Fig. 3. DMD amplitudes calculated from (25) versus Strouhal numbers of flow past a cylinder at the equilibrium state of $Re = 60$. Five dominant DMD modes from DMD and DMD with criterion techniques and their orders are marked. (a) DMD. (b) DMD with criterion.

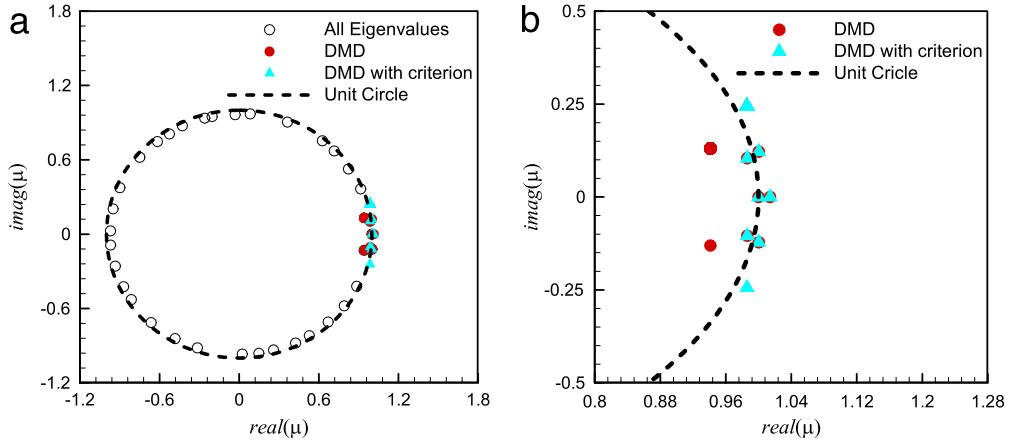


Fig. 4. Eigenvalues of five dominant DMD modes by DMD and DMD with criterion techniques, where the eigenvalues are the same and only the selected dominant eigenvalues are different. Snapshots are collected from flow past a cylinder at the equilibrium state of $Re = 60$. (a) Eigenvalues. (b) Close-up view.

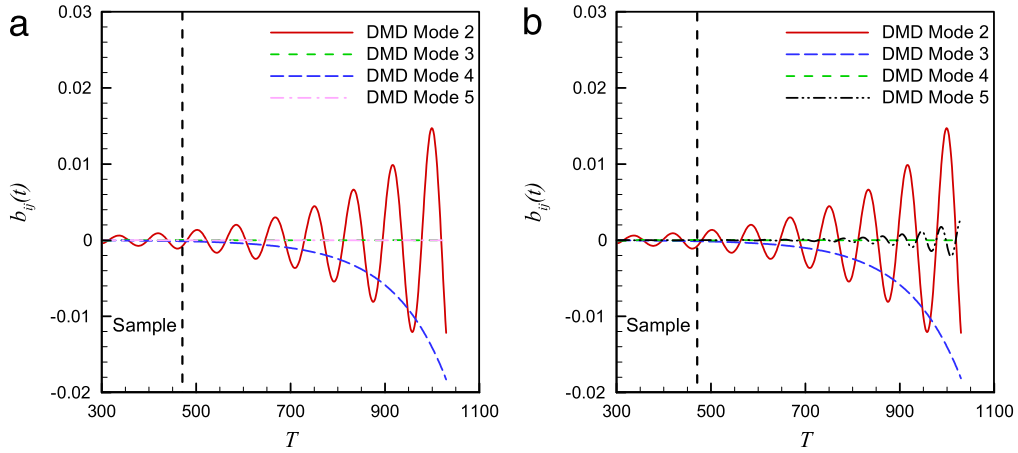


Fig. 5. Evolution of the time coefficients among five dominant normalized DMD modes (real part). Snapshots are collected from flow past a cylinder at the equilibrium state of $Re = 60$. (a) DMD. (b) DMD with criterion.

dataset should be considered. Parametrized DMD proposed by Sayadi et al. [21] redefined the amplitude as a time-dependent coefficient. Inspired by their study, we provide an effective and universal methodology to select dominant DMD modes. Both the initial condition and the temporal evolution of each DMD mode are considered for evaluating each mode's contribution, and a simple criterion suitable for different expressions of DMD is developed. Flow fields decomposed from DMD by introducing

either the companion matrix or the similar matrix can be described as the superposition of each normalized DMD mode and its time coefficient. A parameter defined as the time integration of the normalized time coefficient is introduced to scale the dominance of each DMD mode within the whole dataset, and to rank the dominant DMD modes. This criterion captures important modes for periodic or linear flows like standard DMD technique, and a

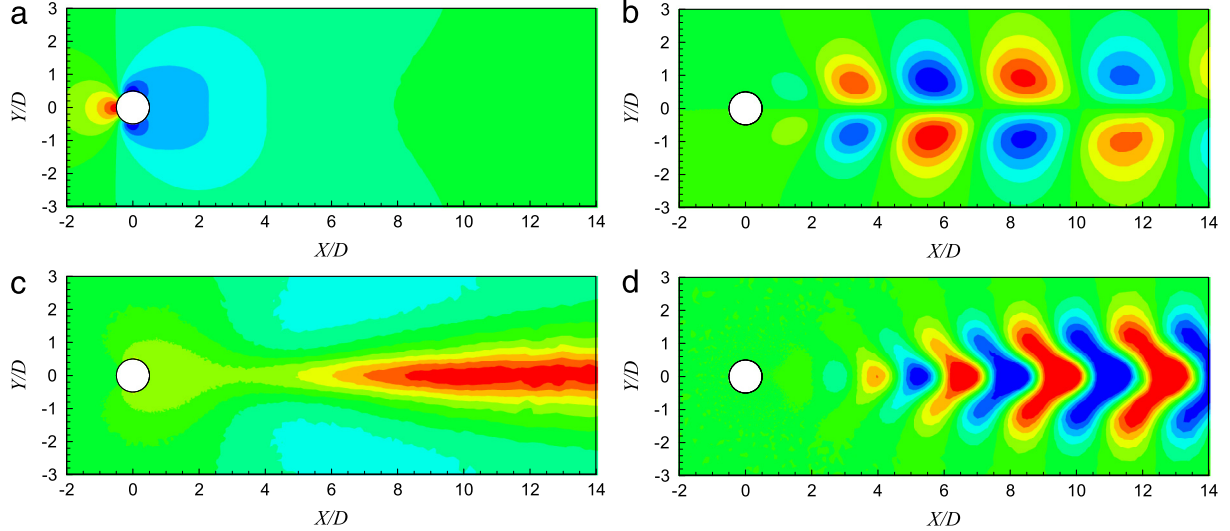


Fig. 6. Dominant DMD modes from DMD with criterion technique of a cylinder at the equilibrium state of $Re = 60$, where the DMD modes are the same as standard method and only the selected dominant DMD modes are different. (a) Mode 1. (b) Mode 2. (c) Mode 3. (d) Mode 5.

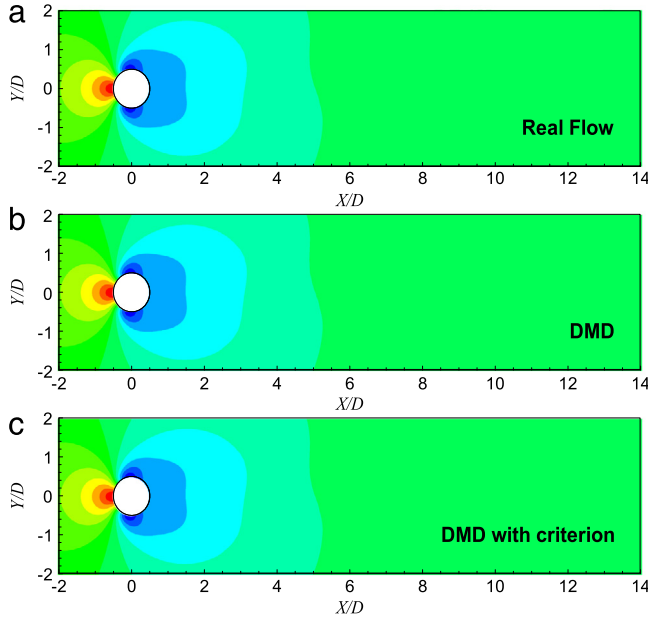


Fig. 7. Pressure field reconstruction at nondimensional time 451.6 of flow past a cylinder at the equilibrium state of $Re = 60$. (a) Flow given by CFD solver. (b) Flow given by DMD. (c) Flow given by DMD with criterion.

better flow reconstruction in unstable or transient flows can be obtained as well.

This paper is organized as follows. In Section 2, two typical DMD techniques based on the companion matrix and the similar matrix are described, and the flow reconstruction process given by these two approaches are described. For the completeness of current study, the sparsity-promoting variant of standard DMD approach is introduced as well. Section 3 generalizes the two standard DMD approaches and derives the criterion for mode selection. Three cases generated from computational fluid dynamics (CFD) simulations are adopted to test the criterion in Section 4, along with the analysis of convergence and sensitivity as mode number increases. A cylinder at $Re = 60$ under equilibrium and transient states and a transonic buffet behavior of a NACA0012 airfoil in the transient regime are studied. Conclusions are summarized in Section 5.

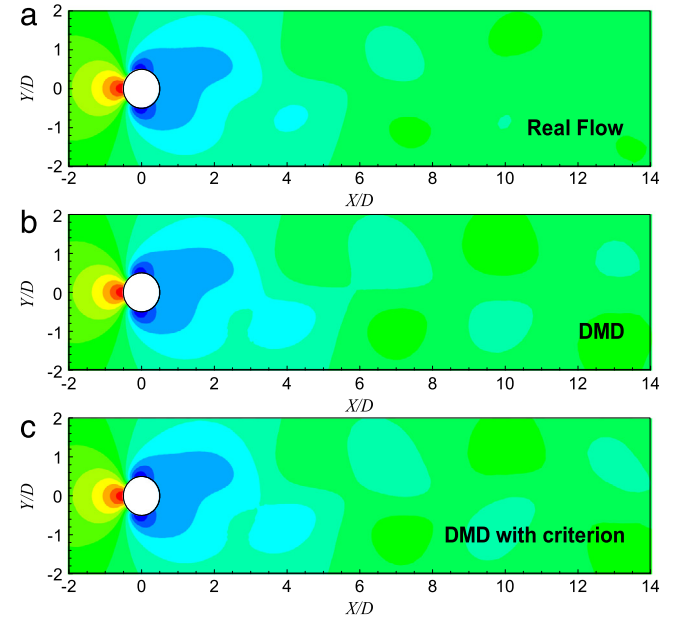


Fig. 8. Pressure field prediction at nondimensional time 1019.6 of flow past a cylinder at the equilibrium state of $Re = 60$. (a) Flow given by CFD solver. (b) Flow given by DMD. (c) Flow given by DMD with criterion.

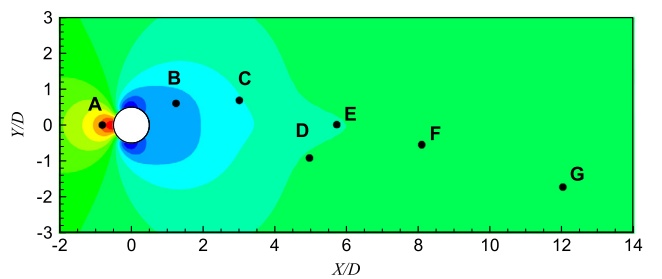


Fig. 9. Mean pressure field of flow past a cylinder at the sampled transient state ($Re = 60$).

2. Dynamic mode decomposition

Model order reduction achieved by DMD can be described by two types of mathematical expressions: the first expression is

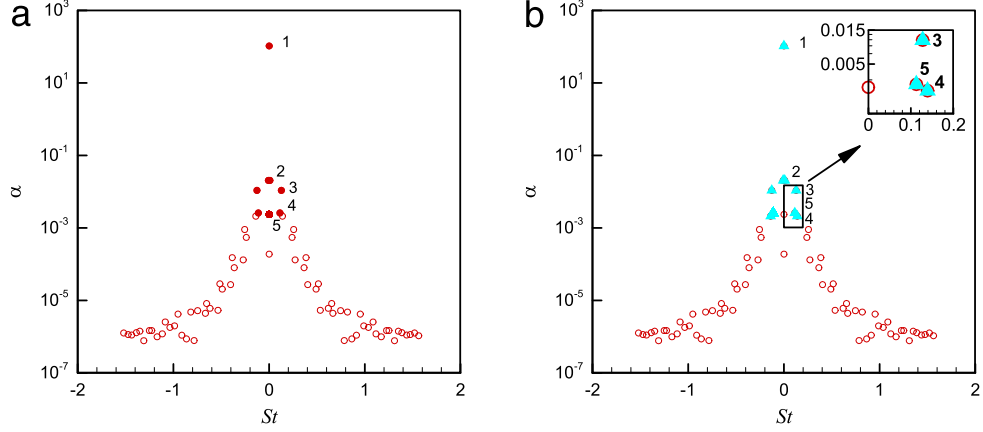


Fig. 10. DMD amplitudes calculated from (25) versus Strouhal numbers of flow past a cylinder at the transient state of $Re = 60$. Five dominant DMD modes from DMD and DMD with criterion techniques and their orders are marked. (a) DMD. (b) DMD with criterion.

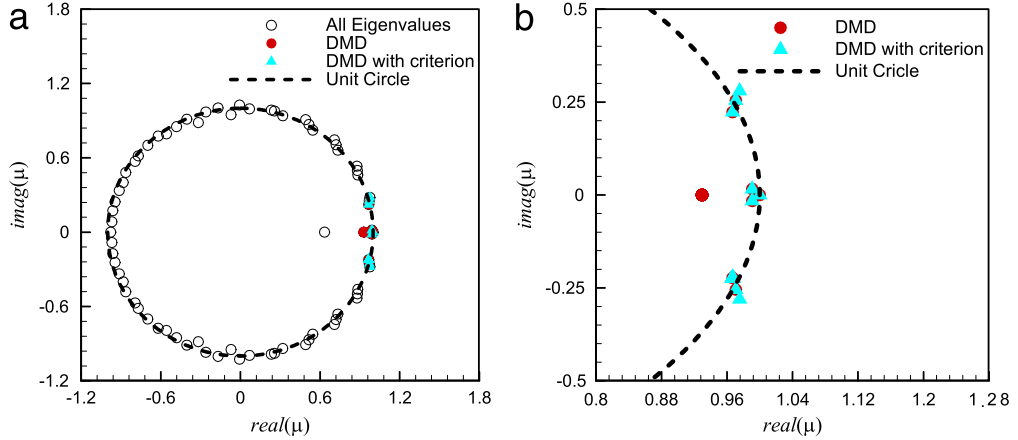


Fig. 11. Eigenvalues of five dominant DMD modes by DMD and DMD with criterion techniques, where the eigenvalues are the same and only the selected dominant eigenvalues are different. Snapshots are collected from flow past a cylinder at the transient state of $Re = 60$. (a) Eigenvalues. (b) Close-up view.

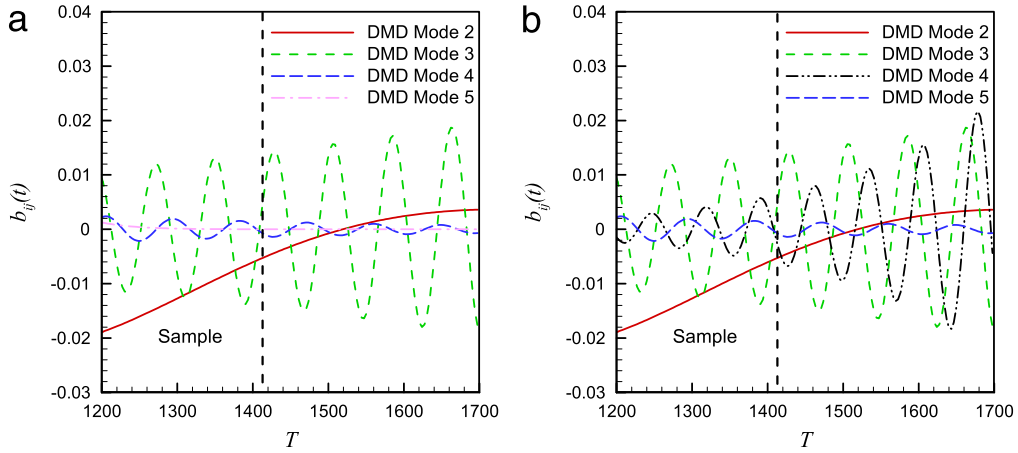


Fig. 12. Evolution of the time coefficients among five dominant normalized DMD modes (real part). Snapshots are collected from flow past a cylinder at the transient state of $Re = 60$. (a) DMD. (b) DMD with criterion.

based on the assumption of linear dependency beyond a critical number of snapshots and a companion matrix is introduced to approximate the infinite-dimensional linear Koopman operator [46, 47]; the latter one is described by adopting a similar matrix to project the linear operator onto a POD basis given by singular value decomposition (SVD) of the snapshot matrix. Both approaches can be used for flow reconstruction, and the latter description is usually more robust in numerical calculation.

2.1. DMD described by the companion matrix

A snapshot sequence with N samples from experiments or numerical simulations is described as $\{\mathbf{x}_1, \mathbf{x}_2, \mathbf{x}_3, \dots, \mathbf{x}_N\}$, where the i th snapshot is $\mathbf{x}_i \in \mathbb{C}^M$, and the time step between two samples is Δt . We assume a linear dynamical system for mapping the current flow field to the subsequent flow field:

$$\mathbf{x}_{i+1} = \mathbf{A}\mathbf{x}_i \quad (1)$$

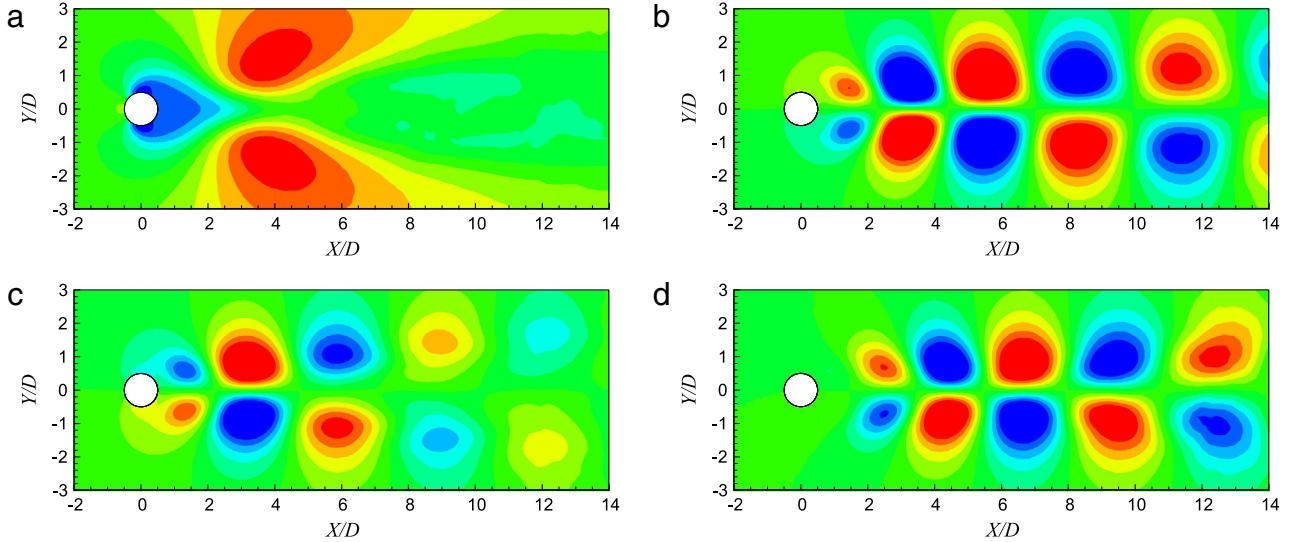


Fig. 13. Dominant DMD modes from DMD with criterion technique of a cylinder at the transient state of $Re = 60$, where the DMD modes are the same as standard method and only the selected dominant DMD modes are different. (a) Mode 2. (b) Mode 3. (c) Mode 4. (d) Mode 5.

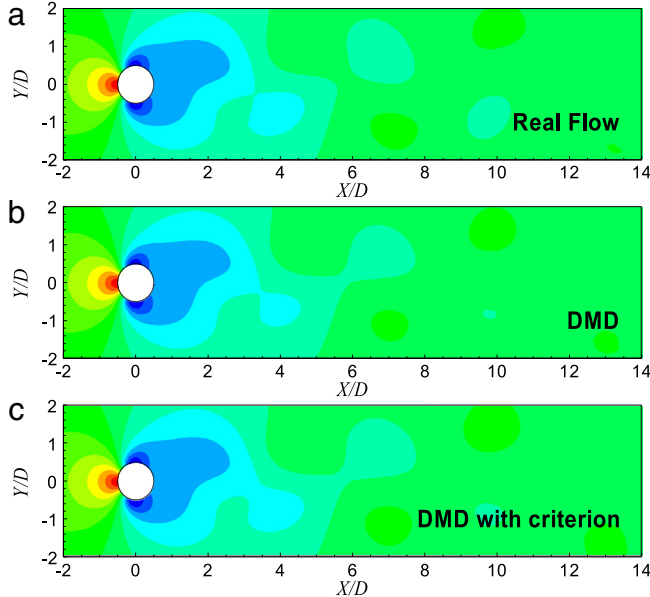


Fig. 14. Pressure field reconstruction at nondimensional time 1256 of flow past a cylinder at the transient state of $Re = 60$. (a) Flow given by CFD solver. (b) Flow given by DMD. (c) Flow given by DMD with criterion.

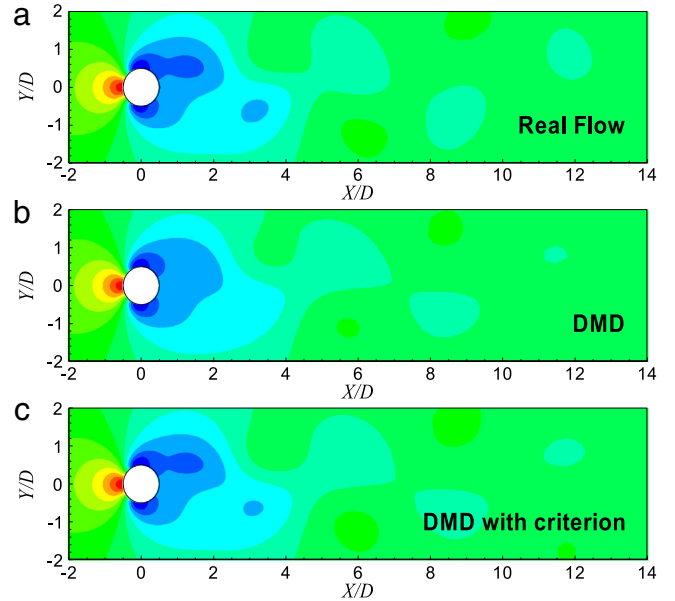


Fig. 15. Pressure field prediction at nondimensional time 1473.6 of flow past a cylinder at the transient state of $Re = 60$. (a) Flow given by CFD solver. (b) Flow given by DMD. (c) Flow given by DMD with criterion.

Table 2
Dominant DMD modes of the transient state from DMD and DMD with criterion approaches.

DMD			DMD with criterion		
Mode	Growth rate	St	Mode	Growth rate	St
1	0	0	1	0	0
2	-2.8406×10^{-3}	0.0080	2	-2.8406×10^{-3}	0.0080
3	1.1178×10^{-3}	0.1275	3	1.1178×10^{-3}	0.1275
4	-2.4455×10^{-3}	0.1128	4	4.6139×10^{-3}	0.1391
5	-2.2840×10^{-2}	0	5	-2.4455×10^{-3}	0.1128

where $\mathbf{A} \in \mathbb{C}^{M \times M}$ is the system matrix containing a particularly large number of entries. If the dynamical system is nonlinear, this assumption is indeed a linear tangent approximation. Because linear relationship is assumed, the dynamical characteristics are contained in the eigenvalues of matrix \mathbf{A} . In order to obtain dominant eigenvalues accurately, the order of the high-

dimensional system matrix \mathbf{A} should be reduced. We then form two matrices:

$$\mathbf{X} = [\mathbf{x}_1, \mathbf{x}_2, \mathbf{x}_3, \dots, \mathbf{x}_{N-1}] \quad (2)$$

$$\mathbf{Y} = [\mathbf{x}_2, \mathbf{x}_3, \mathbf{x}_4, \dots, \mathbf{x}_N]. \quad (3)$$

Using the linear process in (1), a matrix constructed as a Krylov sequence is obtained:

$$\mathbf{Y} = [\mathbf{x}_2, \mathbf{x}_3, \mathbf{x}_4, \dots, \mathbf{x}_N] = [\mathbf{A}\mathbf{x}_1, \mathbf{A}\mathbf{x}_2, \mathbf{A}\mathbf{x}_3, \dots, \mathbf{A}\mathbf{x}_{N-1}] = \mathbf{AX}. \quad (4)$$

When the snapshot number N is beyond a critical value, the subsequent flow field can be expressed as a linear combination of the previous snapshots, indicating that the snapshots become linearly dependent:

$$\mathbf{x}_N = c_1\mathbf{x}_1 + c_2\mathbf{x}_2 + c_3\mathbf{x}_3 + \dots + c_{N-1}\mathbf{x}_{N-1} = \mathbf{xc}. \quad (5)$$

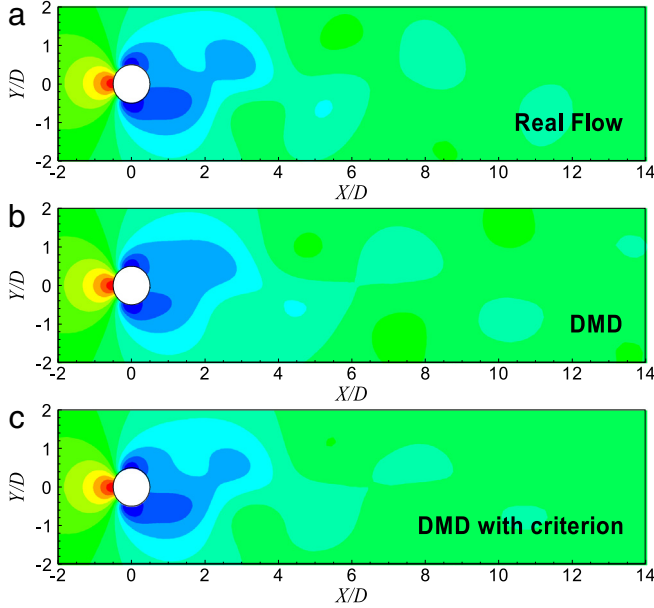


Fig. 16. Pressure field prediction at nondimensional time 1652.8 of flow past a cylinder at the transient state of $Re = 60$. (a) Flow given by CFD solver. (b) Flow given by DMD. (c) Flow given by DMD with criterion.

Thus, we have:

$$\mathbf{A}\mathbf{X} = \mathbf{Y} = \mathbf{X}\mathbf{S} \quad (6)$$

where \mathbf{S} is a companion matrix:

$$\mathbf{S} = \begin{bmatrix} 0 & c_1 \\ 1 & 0 & c_2 \\ . & . & . \\ 1 & 0 & c_{N-2} \\ 1 & c_{N-1} \end{bmatrix} \in \mathbb{C}^{N-1 \times N-1}. \quad (7)$$

From (7), only vector \mathbf{c} includes the unknown quantities, and we can further calculate \mathbf{c} through minimizing the residual vector \mathbf{r} :

$$\mathbf{r} = \mathbf{x}_N - \mathbf{X}\mathbf{c}. \quad (8)$$

When the vector \mathbf{c} is decided by making \mathbf{r} orthogonal to span $\{\mathbf{x}_1, \mathbf{x}_2, \mathbf{x}_3, \dots, \mathbf{x}_{N-1}\}$, eigenvalues of matrix \mathbf{S} approximate the eigenvalues of full-order matrix \mathbf{A} . Compared with matrix \mathbf{A} , matrix \mathbf{S} represents the reduced-order system matrix. The eigenvalues and eigenvectors of \mathbf{S} are given by:

$$\mathbf{S} = \mathbf{T}^{-1}\mathbf{A}\mathbf{T}, \quad \mathbf{A} = \text{diag}(\lambda_1, \dots, \lambda_{N-1}) \quad (9)$$

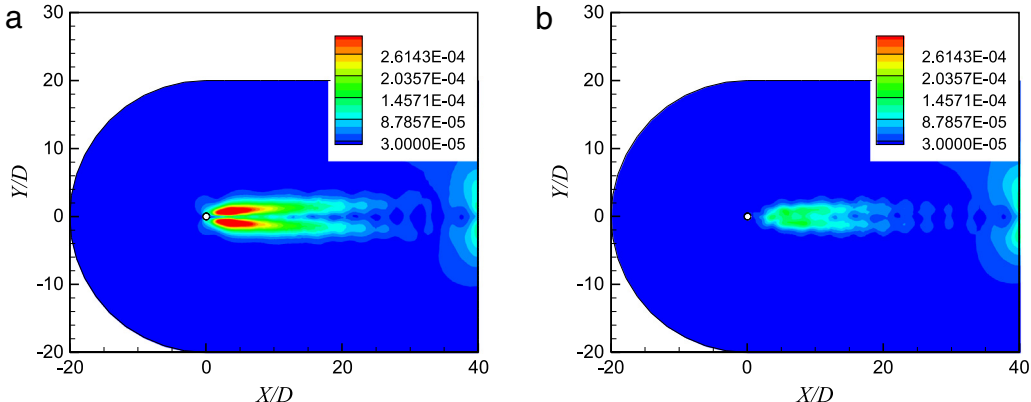


Fig. 17. Mean squared error contour in the predicted flow regime of flow past a cylinder at the transient state of $Re = 60$. (a) DMD. (b) DMD with criterion.

where \mathbf{A} contains eigenvalues in its diagonal and eigenvectors are columns of \mathbf{T}^{-1} . The DMD modes \mathbf{d}_j are defined as columns of matrix \mathbf{D} , where $\mathbf{D} = \mathbf{XT}^{-1}$. As shown in Ref. [7], the flow can be constructed by:

$$\mathbf{x}_k = \sum_{j=1}^m \lambda_j^k \mathbf{d}_j. \quad (10)$$

The matrix form of (10) is given by:

$$\mathbf{X} = [\mathbf{x}_1, \dots, \mathbf{x}_m] = \mathbf{DT} = [\mathbf{d}_1, \dots, \mathbf{d}_m] \begin{bmatrix} 1 & \lambda_1 & \cdot & \lambda_1^{m-1} \\ 1 & \lambda_2 & \cdot & \lambda_2^{m-1} \\ \cdot & \cdot & \cdot & \cdot \\ 1 & \lambda_m & \cdot & \lambda_m^{m-1} \end{bmatrix} \quad (11)$$

where $\tilde{\mathbf{T}}$ is a Vandermonde matrix which is able to diagonalize the companion matrix \mathbf{S} as long as the eigenvalues are distinct. If this is the case, $\tilde{\mathbf{T}}$ will be a precise approximation of matrix \mathbf{T} in (9) and so $\mathbf{D} = \mathbf{XT}^{-1}$. Based on the mathematical relation given by (11), a flow field at any time instant can be approximated by (10) with m dominant DMD modes.

2.2. DMD described by the similar matrix

If DMD is achieved by a similarity transformation of the system matrix, a similar matrix $\tilde{\mathbf{A}}$ should be constructed to replace the full-order matrix \mathbf{A} . Firstly, we seek an invertible matrix by performing SVD on the snapshot matrix \mathbf{X} :

$$\mathbf{X} = \mathbf{U}\Sigma\mathbf{V}^H \quad (12)$$

$$\mathbf{A} = \mathbf{U}\tilde{\mathbf{A}}\mathbf{U}^H \quad (13)$$

where Σ contains r non-zero singular values $\{\sigma_1, \dots, \sigma_r\}$ in its diagonal. From (12), we have $\mathbf{U}^H\mathbf{U} = \mathbf{I}$, $\mathbf{U} \in \mathbb{C}^{M \times r}$ and $\mathbf{V}^H\mathbf{V} = \mathbf{I}$, $\mathbf{V} \in \mathbb{C}^{r \times N}$. In this study, the SVD process is achieved by an economy-size approach described in [20] and the resulting $r = N - 1$. However, it is important to emphasize that if the data is corrupted by noise, a better truncation rank r of the SVD should be considered [48]. Matrix $\tilde{\mathbf{A}}$ can be calculated by minimizing the Frobenius norm of the difference between \mathbf{Y} and \mathbf{AX} :

$$\underset{\mathbf{A}}{\text{minimize}} \|\mathbf{Y} - \mathbf{AX}\|_F^2. \quad (14)$$

From (12) and (13), (14) is expressed as:

$$\underset{\tilde{\mathbf{A}}}{\text{minimize}} \|\mathbf{Y} - \mathbf{U}\tilde{\mathbf{A}}\Sigma\mathbf{V}^H\|_F^2 \quad (15)$$

\mathbf{A} is then approximated by $\tilde{\mathbf{A}}$:

$$\mathbf{A} \approx \tilde{\mathbf{A}} = \mathbf{U}^H\mathbf{Y}\mathbf{V}\Sigma^{-1}. \quad (16)$$

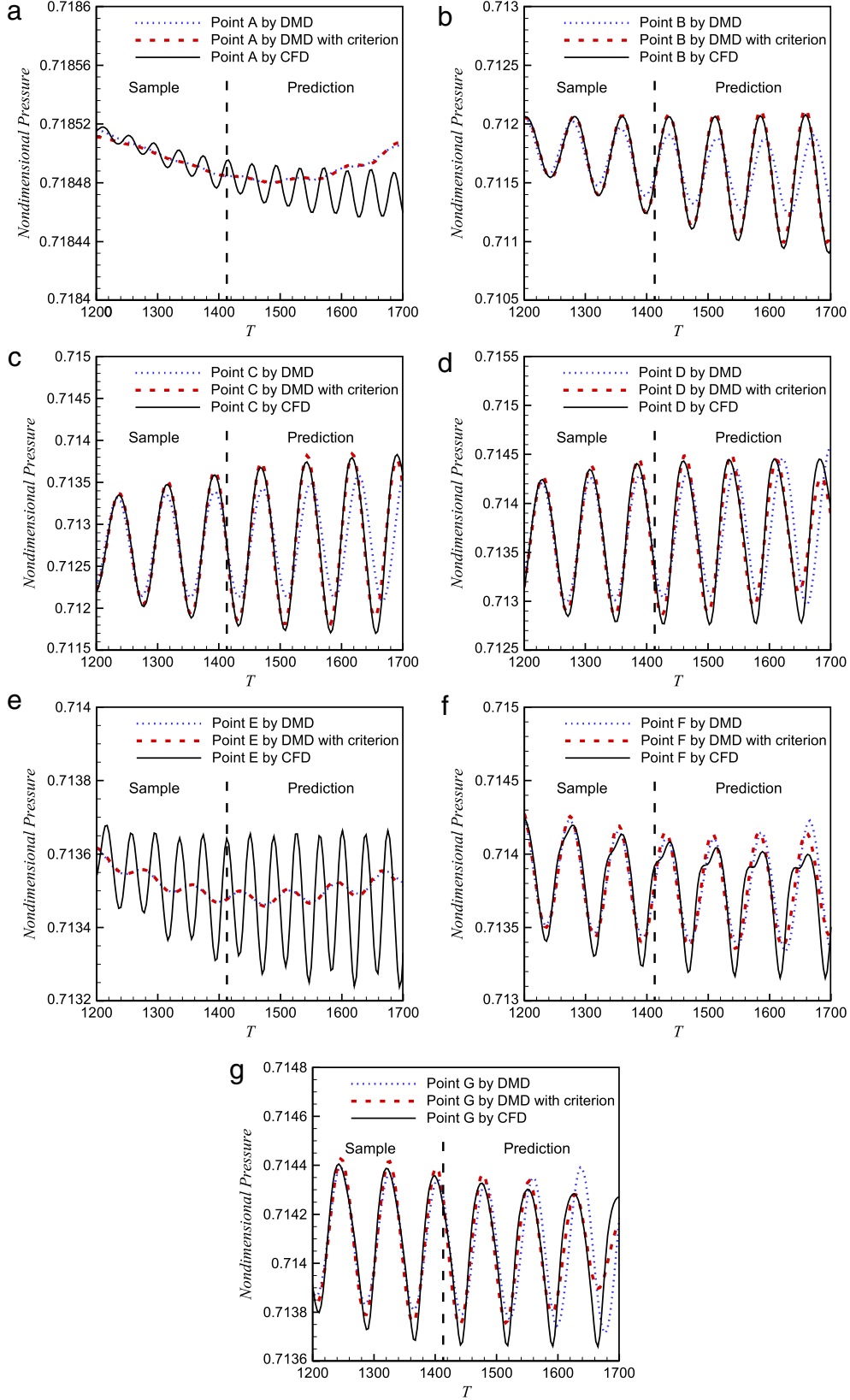


Fig. 18. Temporal evolution of local pressures at seven reference points of flow past a cylinder at the transient state of $Re = 60$. (a) Point A. (b) Point B. (c) Point C. (d) Point D. (e) Point E. (f) Point F. (g) Point G.

Because $\tilde{\mathbf{A}}$ is the similar matrix of \mathbf{A} , eigenvalues of $\tilde{\mathbf{A}}$ are some of eigenvalues of \mathbf{A} . \mathbf{A} has the eigenvalue μ_j which makes $\mathbf{A}\mathbf{w}_j = \mu_j\mathbf{w}_j$, where \mathbf{w}_j is the eigenvector of the j th eigenvalue. The j th dynamic

mode Φ_j is defined as:

$$\Phi_j = \mathbf{U}\mathbf{w}_j. \quad (17)$$

The corresponding growth rate g_j and physical frequency ω_j of this mode are:

$$g_j = \text{Re}\{\log(\mu_j)\}/\Delta t \quad (18)$$

$$\omega_j = \text{Im}\{\log(\mu_j)\}/\Delta t. \quad (19)$$

After the dynamic modes and similar matrix $\tilde{\mathbf{A}}$ are obtained, the evolution of flow fields can be predicted. From SVD, the matrix of POD modes \mathbf{U} can be used to map \mathbf{x}_i into a lower dimensional space:

$$\mathbf{z}_i = \mathbf{U}^H \mathbf{x}_i. \quad (20)$$

Then the system matrix $\tilde{\mathbf{A}}$ can be used for the reduced-order system:

$$\mathbf{z}_{i+1} = \mathbf{U}^H \mathbf{x}_{i+1} = \mathbf{U}^H \mathbf{A} \mathbf{U} \mathbf{z}_i = \tilde{\mathbf{A}} \mathbf{z}_i. \quad (21)$$

If \mathbf{w}_j is the column vector of matrix \mathbf{W} , \mathbf{N} has the eigenvalues in its diagonal:

$$\tilde{\mathbf{A}} = \mathbf{W} \mathbf{N} \mathbf{W}^{-1}, \quad \mathbf{N} = \text{diag}(\mu_1, \dots, \mu_r). \quad (22)$$

The snapshot at any time instant i can be approximated as:

$$\begin{aligned} \mathbf{x}_i &= \mathbf{A} \mathbf{x}_{i-1} = \mathbf{U} \tilde{\mathbf{A}} \mathbf{U}^H \mathbf{x}_{i-1} = \mathbf{U} \mathbf{W} \mathbf{N} \mathbf{W}^{-1} \mathbf{U}^H \mathbf{x}_{i-1} \\ &= \mathbf{U} \mathbf{W}^{i-1} \mathbf{W}^{-1} \mathbf{U}^H \mathbf{x}_1. \end{aligned} \quad (23)$$

Define Φ as the matrix containing each DMD mode Φ_j in its column:

$$\Phi = \mathbf{U} \mathbf{W}. \quad (24)$$

Mode amplitude vector α is represented by:

$$\alpha = \mathbf{W}^{-1} \mathbf{z}_1 = \mathbf{W}^{-1} \mathbf{U}^H \mathbf{x}_1, \quad \alpha = [\alpha_1, \dots, \alpha_r]^T \quad (25)$$

where α_i denotes the amplitude of the i th mode, which represents the modal contribution on the initial snapshot \mathbf{x}_1 . For a standard DMD approach, DMD modes are ordered by their amplitudes (entries of vector α). Substitute (24) and (25) into (23), the flow field at any time instant is given by:

$$\mathbf{x}_i = \Phi \Lambda^{i-1} \alpha = \sum_{j=1}^r \Phi_j (\mu_j)^{i-1} \alpha_j. \quad (26)$$

Matrix \mathbf{X} is then expressed as:

$$\begin{aligned} \mathbf{X} &= [\mathbf{x}_1, \mathbf{x}_2, \mathbf{x}_3, \dots, \mathbf{x}_{N-1}] = \Phi \mathbf{D}_\alpha \mathbf{V}_{and} = [\Phi_1, \Phi_2, \dots, \Phi_r] \\ &\times \begin{bmatrix} \alpha_1 & & & \\ & \alpha_2 & & \\ & & \ddots & \\ & & & \alpha_r \end{bmatrix} \begin{bmatrix} 1 & \mu_1 & \dots & (\mu_1)^{i-1} \\ 1 & \mu_2 & \dots & (\mu_2)^{i-1} \\ \vdots & \ddots & \ddots & \vdots \\ 1 & \mu_r & \dots & (\mu_r)^{i-1} \end{bmatrix}. \end{aligned} \quad (27)$$

In (27), the flow evolution is represented by the Vandermonde matrix \mathbf{V}_{and} , which contains r eigenvalues of the matrix \mathbf{A} . If a smaller number of DMD modes is preferred, the dominant modes can be selected according to their amplitudes described in (25). In summary, for both of the DMD descriptions, a unified approach to select dominant flow modes is needed. This kind of mode selection criterion will be given in Section 3.

2.3. Sparsity-promoting DMD

Since the sparsity-promoting DMD approach [20] is introduced for comparison, we would like to provide a brief introduction to this method here. Sparsity-promoting DMD is a variant of standard DMD approach that combines the tools and ideas from convex optimization with the emerging area of compressive sensing. This method identifies a low-dimensional representation of the unsteady flow in order to capture the most important dynamic

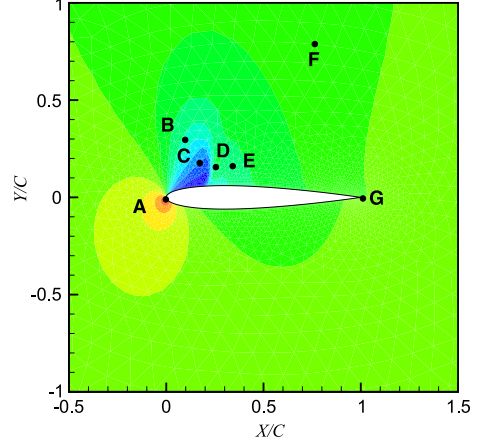


Fig. 19. Transonic buffet flow field at the steady state.

structures through eliminating features that contribute weakly to the data sequence. This is achieved by two steps:

(1) In the first step, a sparsity structure is determined, which achieves a user-defined tradeoff between the number of extracted modes and the approximation error (with respect to the full data sequence). This is described by (28):

$$\underset{\alpha}{\text{minimize}} \quad J(\alpha) + \gamma \sum_{i=1}^r |\alpha_i| \quad (28)$$

where γ is a positive regularization parameter that reflects the emphasis on sparsity of the vector α , and $J(\alpha)$ is the objective function. It is obvious that a larger γ will lead to a sparser solution to (28). Since this problem is a convex optimization problem, the global solution can be obtained by the alternating direction method of multipliers (ADMM) algorithm;

(2) In the second step, the sparsity structure of the vector of amplitudes α is fixed and the non-zero amplitudes are optimized in order to optimally approximate the entire data sequence:

$$\begin{aligned} &\underset{\alpha}{\text{minimize}} \quad J(\alpha) \\ &\text{subject to} \quad \mathbf{E}^T \alpha = 0 \end{aligned} \quad (29)$$

where \mathbf{E} is a matrix that encodes information about the sparsity structure of vector α . This equation can be transformed into a equality-constrained quadratic programming problem and solved by an efficient algorithm described in Appendix C of [20].

Finally, the relationship between the number of selected modes and the loss function that defines the quality of approximation is obtained, and we can further seek a reasonable sparse structure between the quality of approximation and the number of modes. More details about this method are given in [20].

3. Mode selection criterion

For a two-dimensional flow field, DMD approach can be generally described as:

$$\mathbf{x}_i = \sum_{j=1}^{N-1} b_{ij}(t) \Phi_{Norm,j}(x, y) \quad (30)$$

where $\Phi_{Norm,j}$ is the j th dynamic mode normalized by its Frobenius norm with “Norm” representing the word “normalized”, and b_{ij} is the time coefficient of the j th normalized mode at time instant i . In (30), the contribution of each mode to the whole dataset is only decided by its time coefficient b_{ij} . If $|b_{ij}|$ is large, the corresponding mode occupies most of the flow energy at that time instant. Integrating $|b_{ij}|$ in time, a parameter I_j is calculated, which

Table 3

Dominant DMD modes of the buffet behavior at the transient state from DMD and DMD with criterion approaches.

DMD			DMD with criterion		
Mode	Growth rate	k	Mode	Growth rate	K
1	0	0	1	0	0
2	1.9363×10^{-2}	0.1963	2	1.9363×10^{-2}	0.1963
3	-3.7684×10^{-2}	0	3	1.6420×10^{-2}	0
4	1.6420×10^{-2}	0	4	3.4293×10^{-2}	0.1893
5	-7.2770×10^{-1}	0	5	3.0243×10^{-3}	0.3874
6	-8.5522×10^{-2}	0.2412	6	2.2038×10^{-2}	0.3947
7	3.0243×10^{-3}	0.3874	7	-3.7684×10^{-2}	0

denotes the j th dynamic mode's influence on the whole sampling space. I_j is expressed as:

$$I_j = \int |b_j(t)| dt \approx \sum_{i=1}^N |b_{ij}| dt. \quad (31)$$

Our mode selection criterion is to extract dominant DMD modes according to the order of parameter I_j . Compared with previous mode selection approaches, this criterion comprises the temporal evolution of each DMD mode, and some numerically transient modes will not be extracted as the dominant modes. I_j can be calculated with both companion description and similar description of DMD, as shown in (32) and (33), respectively.

$$I_j = \sum_{i=1}^N |(\lambda_j)^{i-1}| \|d_j\|_F^2 \times \Delta t \quad (32)$$

$$I_j = \sum_{i=1}^N |\alpha_j(\mu_j)^{i-1}| \|\Phi_j\|_F^2 \times \Delta t. \quad (33)$$

The proposed criterion is well suited for periodic flows and linear flows, and for unstable or transient systems, this criterion also works well. In this study, DMD equipped with this criterion is called the “DMD with criterion”, whereas the standard DMD is still named as “DMD”. The standard DMD approach used in this study is based on the similar matrix description in Section 2.2, where the dominant modes are selected according to its amplitude defined in (25) and the SVD is performed by an economy-size approach [20]. It should be emphasized that the DMD modes are the same in both approaches but the ordering is different on which basis the dominant modes are selected.

Furthermore, it should be noted that when using the proposed criterion, the user does not need to project the DMD modes on all snapshots because only the variables and vectors described in (32) or (33) are needed (i.e., the norm and eigenvalue of each mode, the amplitude vector described in (25) and the time step). Therefore, the computational cost of DMD equipped with this criterion is not expensive. Also, because in current study, the focus is to extract and rank the DMD modes according to their contribution to the whole dataset, no amplitude optimization [20] or eigenvalue correction [21] is made.

4. Test cases

In order to evaluate the criterion's effectiveness in capturing dominant dynamic modes and reproducing full-order flow fields, two typical flow phenomena (i.e., a cylinder at low Reynolds number and an airfoil buffeting in transonic flow) are used as test cases.

The pressure fields during the temporal evolution of flow are obtained to build the snapshot matrix, and the pressure field changes in time can be predicted after DMD process. Note that flow reconstruction and prediction are different because

reconstruction is to reconstruct the flow field within the sampling dataset $[\mathbf{x}_1, \mathbf{x}_2, \mathbf{x}_3, \dots, \mathbf{x}_N]$ whereas prediction means obtaining the flow field as time evolves beyond the last sampling snapshot \mathbf{x}_N . Because critically stable flow like limit cycle behavior is a standard periodic condition and characteristics of frequency multiplication can be easily obtained by standard DMD approach, this study focuses on the cylinder at equilibrium and transient states where the identification of dominant DMD modes is much more difficult. The Reynolds number $Re = V_\infty D \rho / \mu$ is set to 60, where D , V_∞ , ρ and μ are cylinder diameter, freestream speed, fluid density and dynamic viscosity, respectively. The transonic buffet of a NACA0012 airfoil at $Ma = 0.7$ under transient state is also studied. With the proposed criterion, the dominance of each DMD mode is ordered in a reasonable manner, and high-resolution flow reconstruction and prediction can be achieved by the least number of DMD modes with most of the flow energy. In this study, the cylinder flow is calculated based on laminar Navier-Stokes equations, whereas the transonic buffet is simulated based on unsteady Reynolds-Averaged Navier-Stokes equations with the Spalart-Allmaras (S-A) turbulence model [49]. A CFD solver based on a finite volume method is used, which has been tested in vortex induced vibration investigations [1] and buffet or flutter behavior simulations [50,51]. The hybrid mesh of the cylinder is obtained from [1], and the mesh of the airfoil is the same as that in [50, 51]. Details about numerical algorithms are given in Jiang [52]. The pressure is nondimensionalized by sound speed and density at the far field, whereas the physical time T is nondimensionalized by sound speed and chord length.

4.1. Equilibrium state of flow past a cylinder flow at $Re = 60$

DMD has been utilized to analyze many types of flow around cylinders including one cylinder under low Reynolds number [22, 36], two side-by-side cylinders of different diameters [53] and a near-wall circular cylinder in a flat-plate boundary layer [37]. Chen et al. [22] proposed an optimized DMD approach and analyzed the stability and dynamic modes of a two-dimensional cylinder fluid flow at a Reynolds number of 60. They mentioned that when the mean of the data is subtracted, the DMD is reduced to the temporal discrete Fourier transformation. Since the Hopf bifurcation occurs at $Re = 47$, dynamical parameters of a cylinder flow at $Re = 60$ do not change too drastically, and the behavior from the equilibrium to the limit cycle is easily captured. The development of a cylinder from the unstable steady solution to the ultimate limit-cycle state can be divided into three parts called equilibrium, transient and limit cycle [22]. In Fig. 1, the lift coefficient versus nondimensional time is shown, along with the selected sampling range and prediction range. To trace the frequency change in temporal evolution, nondimensional Strouhal number is used:

$$St = \frac{fD}{V_\infty} \quad (34)$$

where f is the oscillating frequency. When the absolute value of lift coefficient is plotted in logarithm scale, the change in peak value agrees with the change of St in time, as shown in Fig. 2. According to the temporal development of St , three typical states can be identified. It should be noted that Bagheri [47] divided this process into four parts where the transient state is divided into the algebraic growth and the exponential relaxation states. In the unstable equilibrium state, the perturbation is small, and the flow varies in a linear fashion; as flow evolves to the transient regime, a dynamically nonlinear process arises, which makes transient flow the most difficult state to analyze. The transient regime exists in many physical phenomena, like a thermo-acoustic process of an unstable ducted flame [21], so it is important to understand the

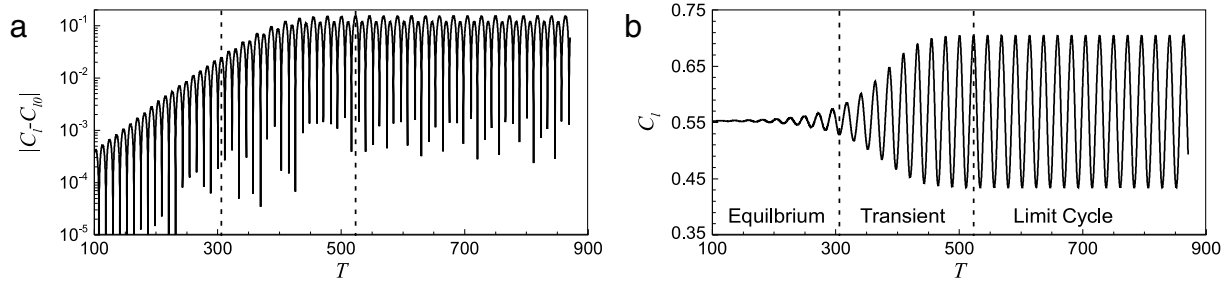


Fig. 20. Lift coefficient response of a NACA0012 airfoil in transonic flow from an unstable steady solution to the limit cycle. (a) Abstract value of the difference between lift coefficient and steady lift coefficient changes with time. (b) Lift coefficient versus nondimensional time.

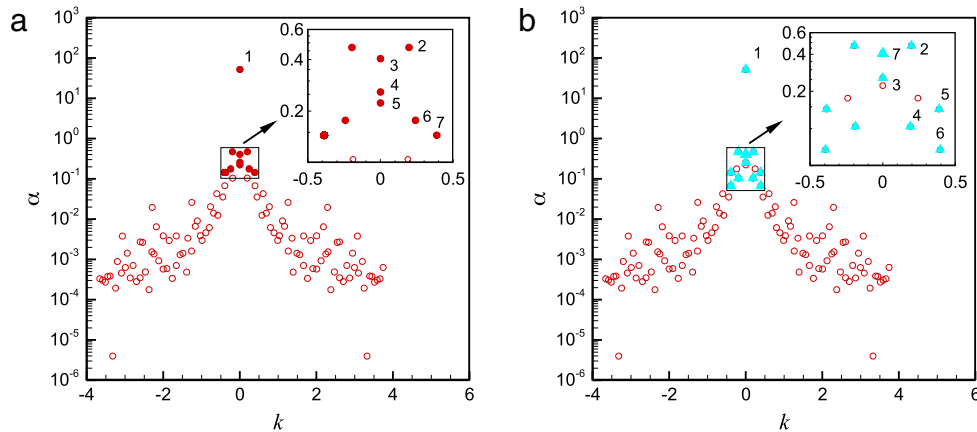


Fig. 21. DMD amplitudes calculated from (25) versus Strouhal numbers of a transonic NACA0012 airfoil at the transient state. Seven dominant DMD modes from DMD and DMD with criterion techniques and their orders are marked. (a) DMD. (b) DMD with criterion.

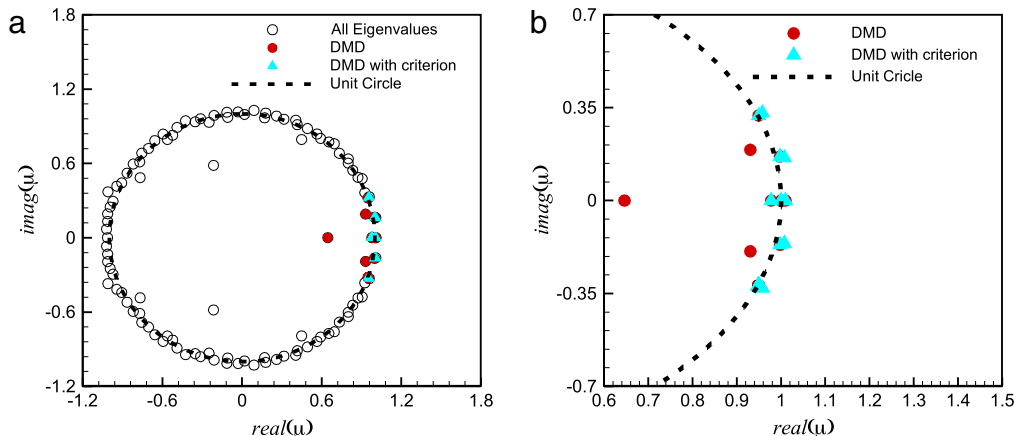


Fig. 22. Eigenvalues of seven dominant DMD modes by DMD and DMD with criterion techniques, where the eigenvalues are the same and only the selected dominant eigenvalues are different. Snapshots are collected from the transient state of a NACA0012 airfoil in transonic flow. (a) Eigenvalues. (b) Close-up view.

complex mechanisms in this regime. For periodic limit cycle state, using DMD will capture the nonlinear dynamics very well [54].

To study the unstable linear dynamics existing in a cylinder flow, the unstable equilibrium regime (case A) with 105 snapshots from $T = 302.8$ to $T = 469.2$ in sampling dataset is firstly analyzed. The Strouhal number at each time instant is calculated by the lift coefficient responses in Fig. 1. As shown in Fig. 2(b), frequency characteristics do not change in the equilibrium state. Mode decomposition is achieved by DMD and DMD with criterion, respectively, and first five dynamic modes are chosen for stability analysis and flow reconstruction. The amplitudes obtained from (25) versus Strouhal numbers is shown in Fig. 3, where the selected modes and their orders are marked. The five dominant eigenvalues from two approaches are shown in Fig. 4, and the corresponding

frequency and growth rate are shown in Table 1. Because the first mode has the eigenvalue close to 1 and is close to the mean of the dataset, it possesses the largest amplitude. Another dominant mode is the oscillating mode characterizing the basic frequency of the equilibrium flow. These two modes can be captured by both standard DMD and DMD with criterion since they are much larger in value compared with other modes. From Table 1, the order of mode 3 and mode 4 exchanges and the shift mode [5] with zero frequency, which represents the change in mean flow, becomes more important in DMD with criterion method. Mode 5 from standard DMD is a typical numerically transient mode since the decay rate is very large, and it decays to zero very fast. As for DMD with criterion, a dynamically unstable mode whose frequency is twice of the flow characteristic frequency is captured. Temporal

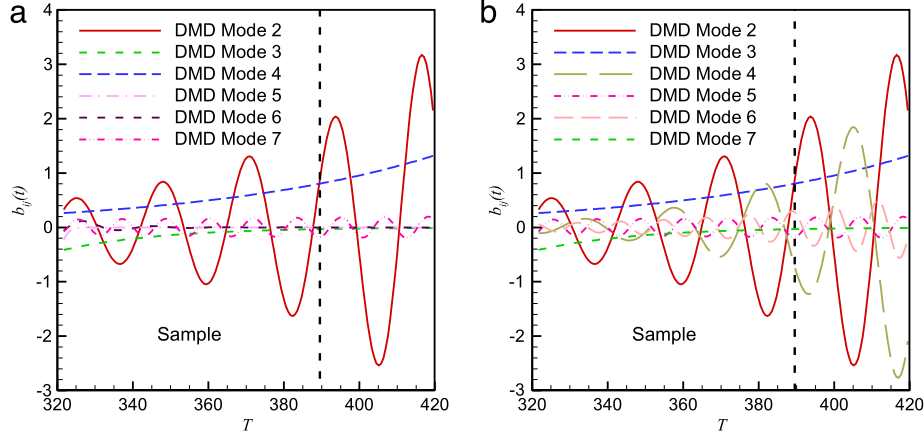


Fig. 23. Evolution of the time coefficients among seven dominant normalized DMD modes (real part). Snapshots are collected from the transient state of a NACA0012 airfoil in transonic flow. (a) DMD. (b) DMD with criterion.

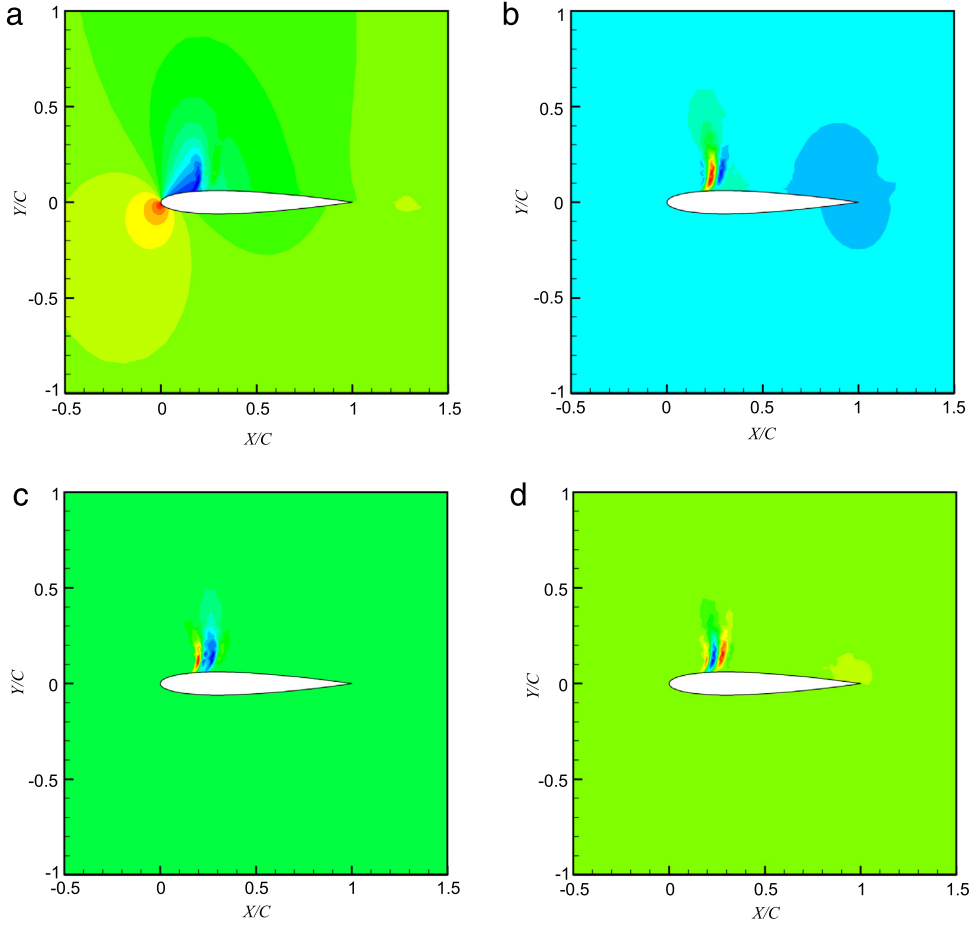


Fig. 24. First four dominant DMD modes from DMD with criterion technique of a NACA0012 airfoil at the transient state, where the DMD modes are the same as standard method and only the selected dominant DMD modes are different. (a) Mode 1. (b) Mode 2. (c) Mode 3. (d) Mode 4.

evolution of each dominant mode's time coefficient is shown in Fig. 5. From Fig. 5, the influence of shift mode (mode 3 of DMD with criterion) is important, and mode 5 of DMD with criterion also contributes to the sampled and predicted flow fields.

Four dominant DMD modes from DMD with criterion technique are shown in Fig. 6. Mode 4 is not given since it only contains the pressure difference near the far field and decays slightly. We then focus on the flow reconstruction by five dominant modes. Figs. 7 and 8 show the flow fields at two time instants retained from dominant DMD modes. Pressure distribution at time instant

451.6, which is within the sampling dataset, is shown in Fig. 7. Flow prediction at time instant 1019.6 is shown in Fig. 8. From Fig. 7(a) and (c), the flow reconstruction has nearly no error compared with that of CFD method, indicating that the selected modes are able to retain the main dynamic characteristics in the sampled dataset. Also for flow reconstruction from standard DMD in Fig. 7(b), the results are in good agreement with the corresponding CFD simulations, because the contribution of the missed double-frequency mode is slight. In Fig. 8, although some error near the wake is observed, the unstable features around the

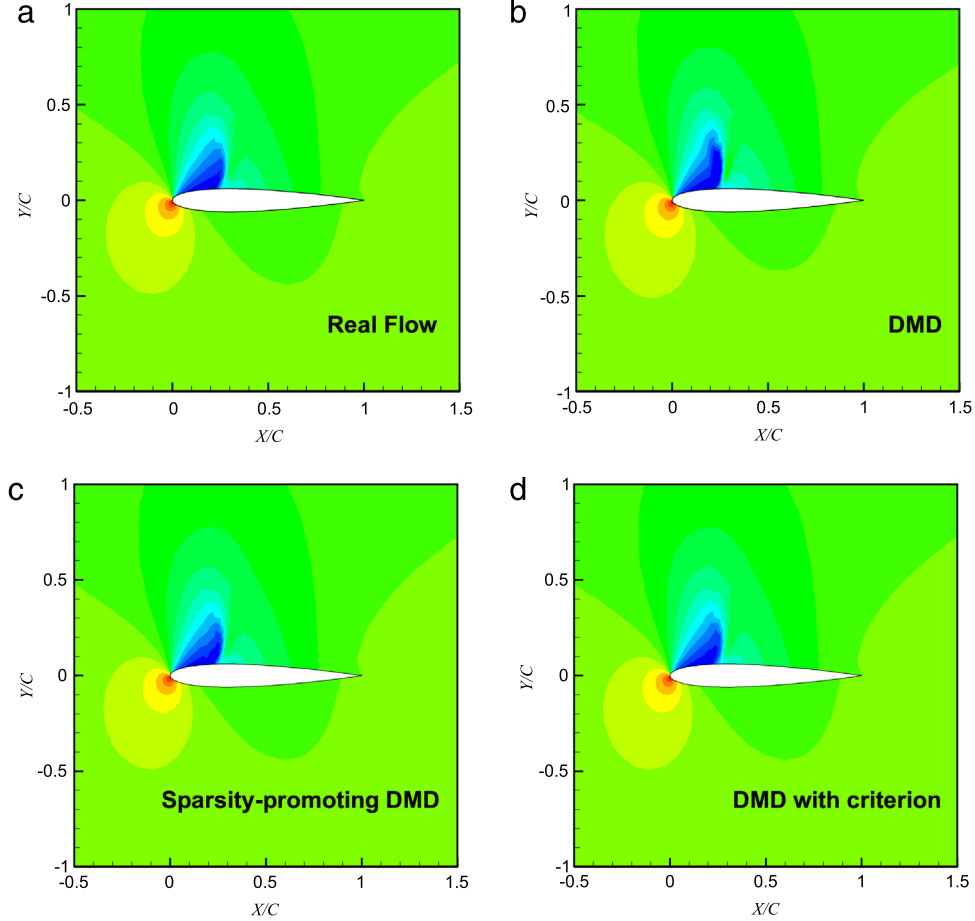


Fig. 25. Flow reconstruction at nondimensional time 385.3 of a transonic NACA0012 airfoil at the transient state. (a) Flow given by CFD solver. (b) Flow given by DMD. (c) Flow given by sparsity-promoting DMD. (d) Flow given by DMD with criterion.

cylinder are accurately described. As the double-frequency mode evolves, the flow fields predicted by both approaches become more different, and the proposed DMD with criterion method describes the flow evolution more accurately. Modeling the equilibrium state indicates that the proposed criterion is well suited for capturing dominant dynamics of linear systems.

4.2. Transient state of flow past a cylinder flow at $Re = 60$

Among the three regimes in cylinder flow, the transient regime is the most difficult state to analyze, since this regime is neither in linear dynamics nor in periodic dynamics where DMD yields elegant solutions [22]. Even though the limit cycle oscillations cannot be predicted from samples at the transient state, dynamics within the transient state can be reconstructed. The considered samples and prediction interval are shown in Fig. 1 (case B), where snapshots of three periods with 75 samples from $T = 1172.8$ to $T = 1409.6$ are selected for mode decomposition. The succeeding three periods are chosen for prediction. Fig. 9 provides the mean flow field within the sampling dataset where 7 fixed points are placed to trace the temporal evolution of pressure.

Fig. 10 presents the dominant modes' frequency and amplitude, as well as the orders of dominant dynamic modes. Five main flow modes are picked for analysis and flow reconstruction. The eigenvalue distribution is shown in Fig. 11, and the corresponding frequency and growth rate are shown in Table 2. The first three modes ordered by standard DMD and DMD with criterion are identical. From time coefficient comparison in Fig. 12, mode 2 with a low frequency plays the similar role as the shift mode described

in the equilibrium regime. The third dynamic mode which is close to the flow frequency is a dominant unstable mode. Since the flow has not saturated on the limit cycle state, this mode exhibits the development of the transient state. From Fig. 2(b), the basic frequency changes with time in the transient regime. Therefore, mode 4 given by DMD with criterion is adopted to compensate the frequency change during the flow developments. Unfortunately, this mode is left out by standard DMD method. Mode 5 of DMD with criterion, also mode 4 of DMD, is a decaying dynamic mode whose frequency is close to the basic frequency. But the influence of this mode is not as significant as mode 4 from DMD with criterion in flow prediction, as shown in Fig. 12(b). Mode 5 from standard DMD approach decays to zero very fast, which hardly contributes to the evolution of the cylinder flow. This mode can be categorized into a numerically transient mode.

In Fig. 13, dominant DMD modes obtained by DMD with criterion technique are shown. Since the static mode 1 is close to the mean flow field shown in Fig. 9, only other dynamic modes are given. Compared with the shift mode given in Fig. 6(c), mode 2 in Fig. 13(a) differs in pressure distribution of the wake flow. The subsequent two modes shown in Fig. 13(b) and (c) are analogous near the upper and lower surfaces of the cylinder because they exhibit a vortex shedding behavior. The unstable vortex shedding phenomenon is dominated by these two modes. Mode 5 in Fig. 13(d) is similar to an unstable mode described in Fig. 6(b). Because the vortex shedding exists in the transient regime is not manifested by this mode, it decays as the flow is evolving in time.

After several dominant DMD modes are obtained, the flow reconstruction and prediction are studied. Both the dynamics of

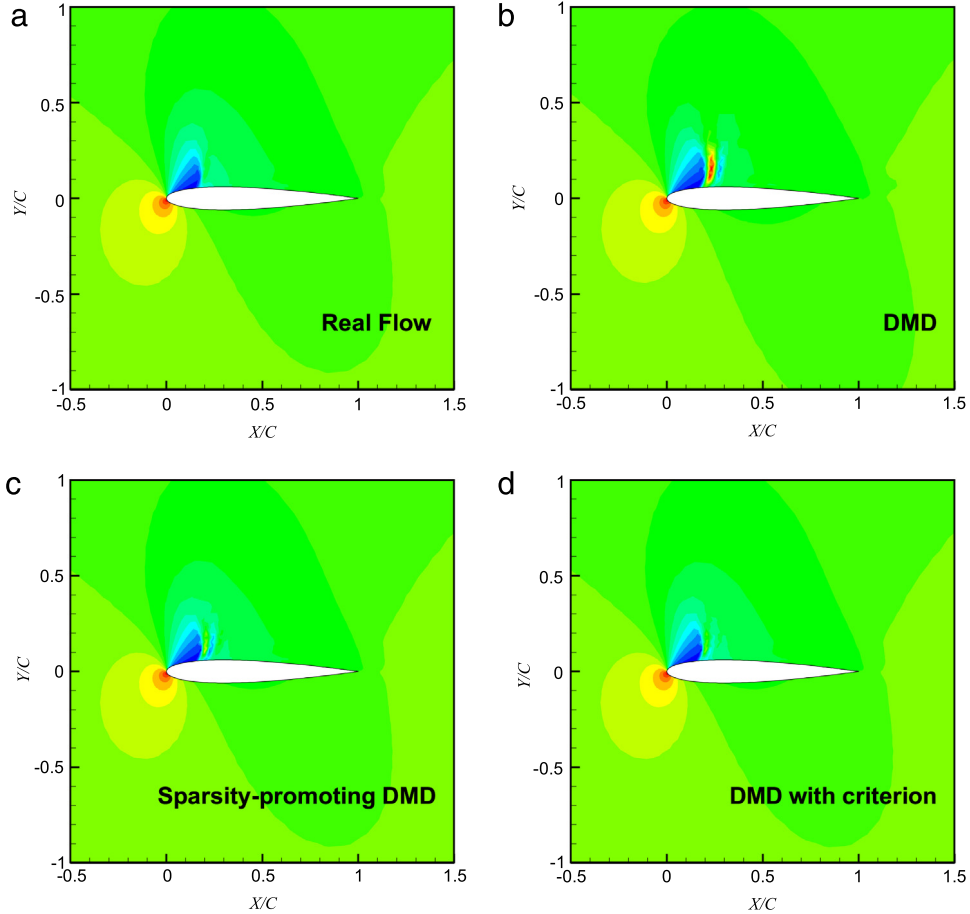


Fig. 26. Flow prediction at nondimensional time 394.9 of a transonic NACA0012 airfoil at the transient state. (a) Flow given by CFD solver. (b) Flow given by DMD. (c) Flow given by sparsity-promoting DMD. (d) Flow given by DMD with criterion.

sampled snapshots and flow field beyond the sampling space are recovered. Flow at nondimensional time 1256 is shown in Fig. 14, where the flow starts to evolve in the transient state and the large-scale vortex shedding does not happen. Because the chosen flow condition is within the sampling dataset and the flow develops very slightly, this state is accurately described by both DMD and DMD with criterion techniques. A pressure field at $T = 1473.6$ is shown in Fig. 15, which is beyond the whole sampling dataset. From Fig. 15(b), flow predicted by DMD fails to exhibit the vortex shedding phenomenon because an important dynamic mode (mode 4 of DMD with criterion) is neglected. But in Fig. 15(c), flow reconstruction by DMD with criterion accurately shows the local pressure difference induced by unsteady vortex shedding. When $T = 1652.8$, as shown in Fig. 16, the cylinder flow is approaching the limit cycle state, thus a stronger vortex shedding is observed. The reconstructed flow by DMD with criterion agrees with the real flow field very well, but the DMD method fails to capture that behavior.

In order to make a comprehensive comparison on the prediction error, the mean squared error mse contour calculated from the real flows and predicted flows is presented in Fig. 17. The definition of mse is given in (35):

$$mse = \sqrt{\frac{1}{N_p} \sum_{i=1}^{N_p} |\mathbf{x}_{CFD}(i) - \mathbf{x}_{DMD}(i)|^2} \quad (35)$$

where N_p is the number of predicted snapshots, $\mathbf{x}_{CFD}(i)$ and $\mathbf{x}_{DMD}(i)$ are the i th snapshot to be predicted from CFD simulations and the DMD approach, respectively. In Fig. 17, as error contours are

scaled to the same value, DMD approach exhibits larger deviations, especially in the wake flow near the cylinder. However, the flow construction by DMD with criterion shown in Fig. 17(b) exhibits smaller overall error than the standard method, indicating that dynamics of a cylinder flow at the transient state is well captured by the DMD method combined with the proposed criterion.

Fig. 18 shows the temporal evolution of pressure at all reference points. Flow evolution in these fixed points indicates the development from the transient state to the saturated limit cycle. As points A and E are near to the symmetric axis of the cylinder, the pressure at these points shows double frequency effects. To capture this behavior, the dynamic modes with double of the basis frequency should be included. However, from a flow approximation perspective, these modes actually contribute little to the flow evolution. Therefore, even though adopting these modes (e.g., the sixth dynamic DMD mode, which is a double-frequency mode with a symmetrical configuration) will further improve the accuracy, these modes are not allowed in current study since using five modes is enough to obtain acceptable accuracy. For points B and C which are close to the cylinder, the DMD with criterion mimics the amplitude of pressure precisely, and nearly no phase difference between the predicted flow and the real flow is observed. When the reference points are a little far from the cylinder, like points D and F, although DMD with criterion is used, some deviations still exist. This is because pressures near these two points manifest nonlinearity induced by the vortex shedding phenomenon, making it hard to reproduce the flow evolution. At point G, some errors are observed, but the change in pressure is also slight. The test case of a transient regime shows that the proposed criterion helps to identify dominant dynamic

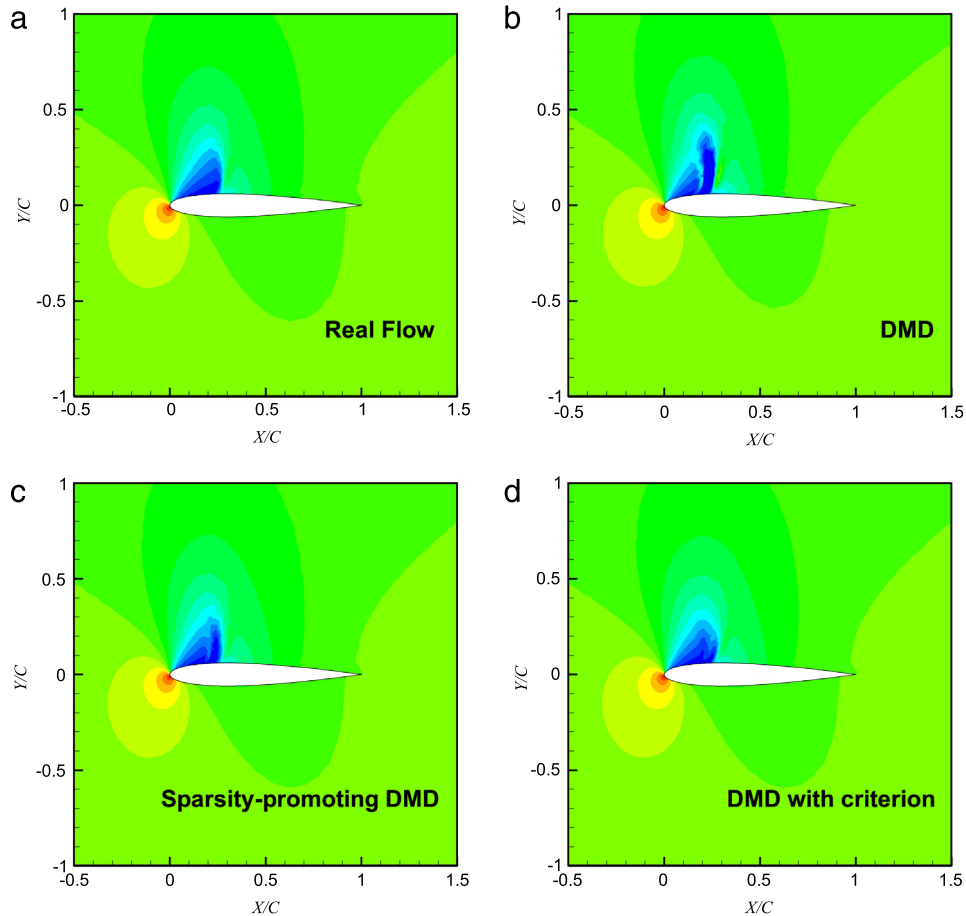


Fig. 27. Flow prediction at nondimensional time 403.3 of a transonic NACA0012 airfoil at the transient state. (a) Flow given by CFD solver. (b) Flow given by DMD. (c) Flow given by sparsity-promoting DMD. (d) Flow given by DMD with criterion.

modes for some unstable nonlinear processes like nonlinear post-bifurcation states.

4.3. Transient state of a transonic NACA0012 airfoil buffet case

Buffet behavior occurred in transonic flow is similar with a cylinder flow at low Reynolds number since it will also develop into a periodic limit cycle oscillation caused by the instability of unsteady flow field. Compared with the cylinder flow, periodic loads during the structure buffeting may cause structural fatigue or even flight accidents. Therefore, it is of great importance to study the mechanism about buffet and understand the nonlinear interactions between shock wave and the boundary layer. Because transonic buffet exhibits some periodic features, using DMD will help to capture the dominant frequency information and stability characteristics, thus permitting further investigations in characteristic analysis or buffet suppression.

A standard buffet case chosen in this paper is a NACA0012 airfoil. The flow conditions are Mach number $Ma = 0.7$, Reynolds number $Re = 3 \times 10^6$, and the mean angle of attack $\alpha_0 = 5.5^\circ$. As shown by Gao et al. [55], the computational buffet onset of a stationary NACA0012 airfoil is 4.8° , so in the selected case, buffet behavior is bound to occur. Analysis of periodic limit cycle states has been studied by Kou et al. [54]. In this study, the unstable transient regime is observed. In order to capture the flow development from steady to unsteady state, an unstable steady solution is needed. We obtain this solution by utilizing closed-loop control methodology described in Gao et al. [55]. Note that this steady solution is a real solution to the unsteady flow and completely satisfies the governing equations and boundary

conditions in mathematical form. This steady state flow is shown in Fig. 19, along with some reference points for tracing the temporal evolution of pressure given by both CFD solver and ROM. The chord length is defined as C . Lift coefficient responses developed from the steady solution are shown in Fig. 20. According to the magnitude of lift coefficient, the flow can also be divided into equilibrium, transient and limit cycle regimes. It should be noted that a difference between unstable buffet flow and a cylinder flow is that the basic frequency does not change drastically as the flow evolves, and the nondimensional reduced frequency $k = \omega b/V_\infty$ stays around 0.195, where ω is the oscillatory frequency and b is the half-chord length. The unstable transient regime with 114 pressure snapshots from $T = 321.7$ to $T = 389.5$ in sampling dataset is analyzed and the end of predicted flow is at $T = 419.5$. Because the flow is in transonic state where strong nonlinear effects induced from moving shock waves and separated flows exist, seven dynamic modes are chosen for modeling flow dynamics.

Amplitudes of seven dominant modes obtained by DMD and DMD with criterion are shown in Fig. 21, where three consecutive modes with zero frequency are captured by the standard method. From eigenvalues depicted in Fig. 22, one of the static modes obtained according to the amplitude has very large decay rate because it is close to the origin. From Table 3, the mode with the largest decay rate is the fifth DMD mode, whereas using DMD with criterion will not extract this mode as a dominant one. From previous study, this mode is a typical numerically transient mode. Besides, from Table 3, all DMD modes from DMD with criterion have positive growth rates except the first and the last static modes. Because the sampling state is just after the equilibrium

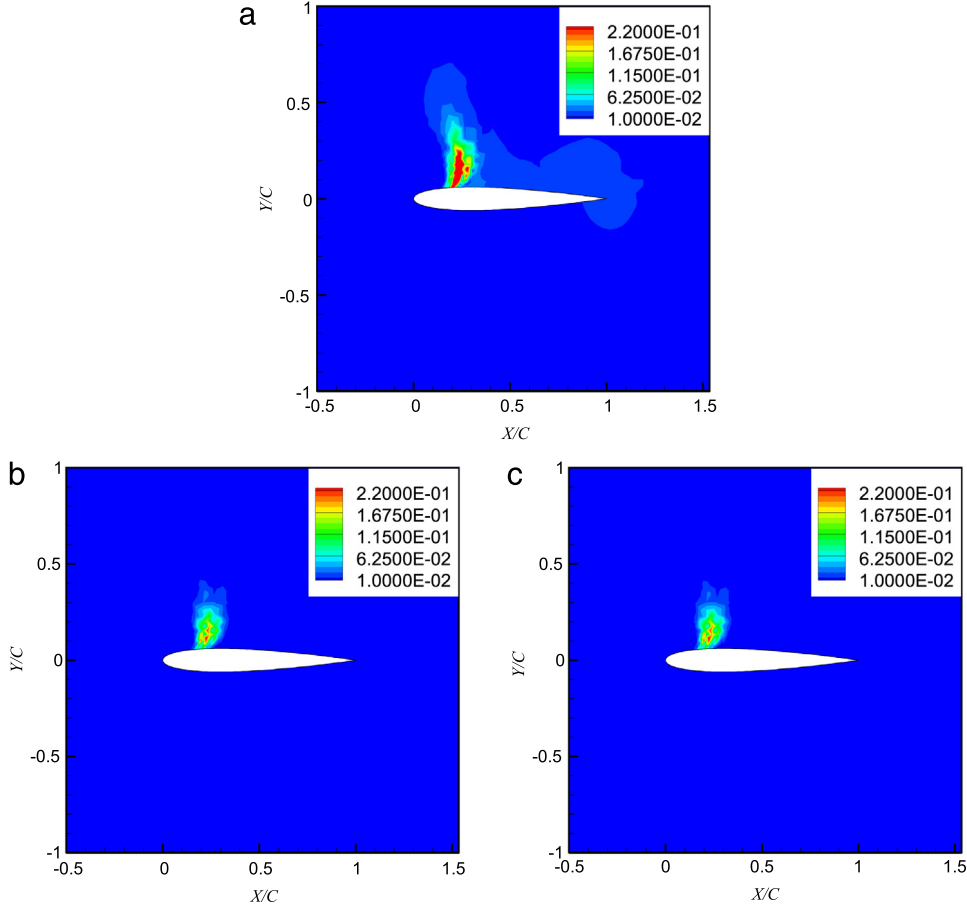


Fig. 28. Mean squared error contour in the predicted transient flow regime of a NACA0012 airfoil in transonic flow. (a) DMD. (b) Sparsity-promoting DMD. (c) DMD with criterion.

regime, it is reasonable that most of the dynamic modes are unstable. In Fig. 23, some numerically transient modes from DMD technique, i.e., mode 3, mode 5 and mode 6, can be easily identified. These modes have very little influence on the prediction interval. However, DMD with criterion only captures one transient mode, i.e., mode 7.

In Fig. 24, first four dominant dynamic modes from DMD with criterion are shown. Static mode 1 is close to the mean flow field but is different from the steady flow shown in Fig. 19, since mean flow is just the time-averaged solution of the unstable process, which is not a real solution [55]. All other modes reflect the oscillating features resulted from shock waves. This indicates that more linear modes are needed to describe the nonlinear characteristics resulted from moving shock wave. Flow reconstructions at \$T = 385.3, 394.9\$ and \$403.3\$ are presented in Figs. 25–27, where the reconstruction within the sampling range is shown in Fig. 25 and the flow predictions are shown in the other figures. Besides, the results are compared with those from sparsity-promoting DMD [20] as well. After the amplitude optimization process by sparsity-promoting DMD, we choose seven conjugate dynamic modes with the regularization parameter \$\gamma = 289.03\$, which are further utilized for model order reduction. In Fig. 25, even though the predicted flow field is one of the sampled data, DMD approach presents some error behind the shock wave, making the edge of the shock wave unsMOOTH. As shown in Fig. 25(c), flow reconstruction by sparsity-promoting DMD also shows small error. Pressure field given by DMD with criterion mimics real flow with higher accuracy. The predicted flow at \$T = 394.9\$ in Fig. 26 is beyond the modeling dataset, where DMD and sparsity-promoting DMD exhibit some pressure

differences near the discontinuous region behind the shock wave. However, the flow reconstructed by DMD with criterion describes the position and the height of the shock wave precisely. As flow evolves to \$T = 403.3\$, shock wave predicted by DMD in Fig. 27(b) is separated into two fractions, which does not agree with the flow field from CFD simulation. Shock wave from sparsity-promoting DMD also begins to separate in Fig. 26(c). Compared with standard and sparsity-promoting approach, results from DMD with criterion is in accordance with those from CFD simulations.

Comparisons of mean squared error *mse* contour in prediction space of all DMD-based methods are given in Fig. 28. From Fig. 28, large errors from all methods mainly exist near the shock wave in transonic flow. Compared with DMD approach, sparsity-promoting DMD and DMD with criterion show smaller errors near the shock wave. In Fig. 29, temporal evolutions at all reference points are shown. These points are either close to the shock wave or near the trailing edge behind the shock wave. At point A, changes of pressure are well captured by sparsity-promoting DMD and DMD with criterion approach. The predicted pressures at point B exhibit no discontinuous manner since this reference point is near to the outer space of shock wave. When it comes to point C, which is in the shock wave regime, all approaches cannot describe the pressure mutation as the shock wave moves. Due to the moving shock wave, pressure at point D has an increasing trend with a non-periodic behavior. But DMD with criterion demonstrates better robustness to this nonlinear behavior. At point E, high-frequency component appears as the shock wave moves. Since point F is far from the shock wave, the pressure exhibits a nearly linear behavior and is well described by sparsity-promoting DMD and DMD with criterion. Temporal trace at point G also follows a linear

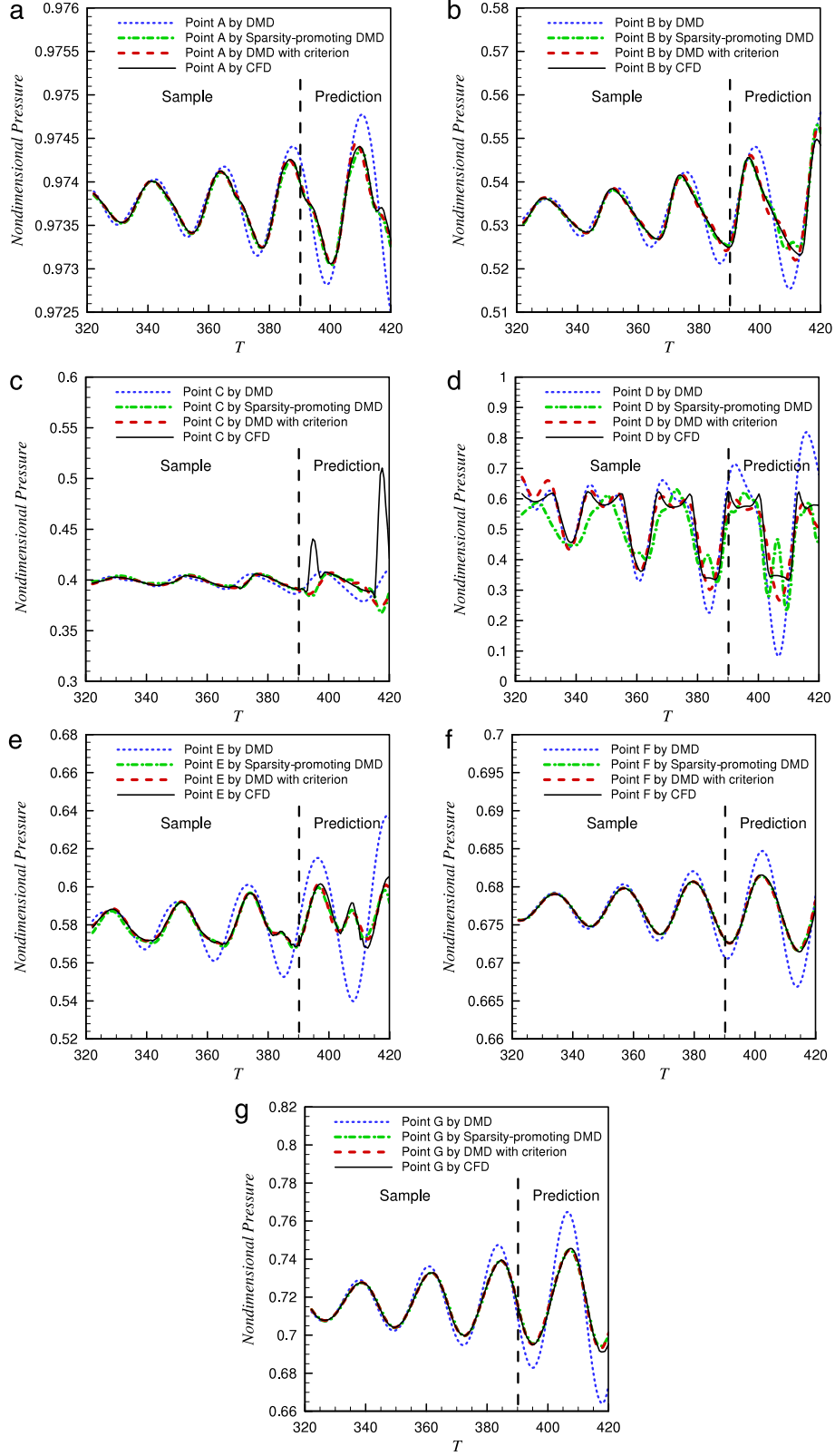


Fig. 29. Temporal evolution of local pressures at seven reference points of a transonic NACA0012 airfoil at the transient state. (a) Point A. (b) Point B. (c) Point C. (d) Point D. (e) Point E. (f) Point F. (g) Point G.

increasing manner because it is at the trailing edge of the airfoil which is far from the shock wave. In Fig. 29, pressure evolution at the above-mentioned points is well depicted by the dominant modes selected from DMD with criterion, and better accuracy from DMD with criterion exists both near the shock wave and

far from it. Furthermore, although sparsity-promoting DMD shows similar performance with DMD with criterion approach at nearly all points, the method with the proposed criterion outperforms the sparsity promoting one at point D, which is near to the shock wave. This transient case indicates that the DMD with criterion

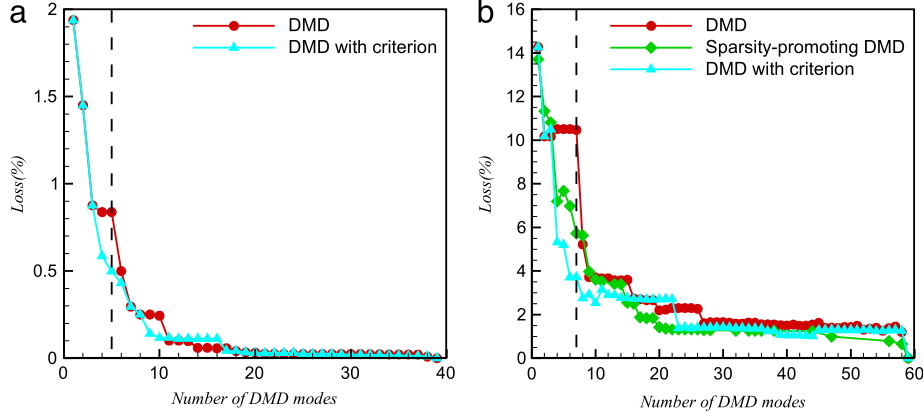


Fig. 30. Loss functions versus number of DMD modes. (a) Flow past a cylinder at the transient state. (b) Buffet case at the transient state.

method outperforms the standard one or the sparsity-promoting approach even though there are nonlinear behaviors like moving shock waves in transonic flow.

4.4. Convergence and sensitivity analysis of the improved approach

Although DMD with criterion has shown better performance in analyzing many types of flows in previous sections, some details about its convergence and sensitivity should be studied for better utilizing this approach. The convergence study is achieved by comparing the approximation error changing with the selected number of DMD modes, whereas the sensitivity is investigated by setting the same sampling size but different initial snapshots and observing the convergence of reconstruction error. The overall error in the whole sampling dataset is scaled by the loss function provided in [20]:

$$\text{loss} = 100 \frac{\|\mathbf{X} - \Phi \mathbf{D}_\alpha \mathbf{V}_{\text{and}}\|_F}{\|\mathbf{X}\|_F}. \quad (36)$$

Fig. 30 compares the loss function versus the number of DMD modes r between the DMD method and the DMD with criterion approach, where the convergence of flow past a cylinder at the transient state is shown in Fig. 30(a) and the convergence of buffet case is shown in Fig. 30(b). The dashed line indicates the loss function obtained by the selected dominant DMD modes in previous test cases. From the loss function change in Fig. 30(a), the decline of overall loss is unsound and two steps with nearly no error descending can be observed between modes 4–5 and modes 8–10. This phenomenon indicates that adding a mode does not contribute to improved accuracy of flow approximation. However, the DMD with criterion method has a smooth decline with increasing number of selected modes, and the error is negligible (less than 0.1%) when the first ten modes are extracted. Increasing the number of selected mode to more than ten, the two methods have small variations. This is reasonable because the remaining DMD modes are predominantly some transient modes used to compensate the residual errors. Since using the first five modes will make the performance loss less than 0.5%, which is small enough, five dominant modes of flow around a circular cylinder are used this study.

Fig. 30(b) demonstrates the error convergence of the transonic buffet case at the transient state. Because of the complex nonlinear features caused by the interactions between the shock wave and the boundary layer, it is difficult to get a smooth descending trend. As selecting the first seven modes by DMD with criterion gives 5% error, which is sufficiently small, these modes are chosen for flow reconstruction in the previous test case. For DMD, the loss function stays unchanged when increasing the number of selected

modes from 4 to 7. Mode 8 and mode 9 from DMD contribute a lot to the error convergence, and DMD with criterion gives preference to these modes, resulting in a faster convergence. The convergence behavior of sparsity-promoting DMD is obtained by setting the range and step of the regularization parameter and then optimizing it through the whole dataset. After that, the relationship between the number of selected modes and the loss function is obtained. Moreover, there is no surprise that the error of sparsity-promoting DMD decreases much more smoothly because it optimizes the amplitudes for a better flow approximation. But DMD with criterion shows its capability in producing accurate flow reconstruction with a smaller number of modes because the sparsity-promoting variant of DMD captures some transient modes with large decay-rate, making the loss function larger at mode number ranging from 5 to 14. Since the proposed criterion sorts DMD modes by each mode's influence on the whole dataset, less modes are needed for capturing dominant flow dynamics. As the number of selected modes increases, all methods reach similar accuracy. But for reduced-order modeling practices, these mode numbers are too large. In most of complex flows, a minority of dominant modes is adequate to construct a low-dimensional model, and this criterion helps to pick out numerically transient modes with large decay rates and identify the most significant flow features for model order reduction.

Another feature of DMD with criterion method is the low sensitivity to initial sampling condition. In order to explain this advantage, loss functions versus numbers of selected DMD modes at different initial times are displayed in Figs. 31 and 32. It should be emphasized that changing the initial condition is achieved by slightly shifting the sampling region and the selected number of samples at different initial conditions are the same. The slight frequency variations with changing initial conditions are due to the basic frequency varying with sampling space, as shown in Fig. 2(b). Sensitivity analysis of the transient cylinder flow and the transient buffet behavior is given in Figs. 31 and 32, respectively. From Fig. 31, a 0.5 percent loss can be obtained by first five modes except DMD utilized at two initial conditions, i.e., $T = 1172.8$ and $T = 1173.6$. The convergence trends by DMD with criterion at different initial conditions are smooth within the first five modes, whereas unsound trends within the dominant modes are observed in DMD. Moreover, with different sampling onsets, the loss functions of DMD are either more than 0.8% or approaching 0.5% with five modes selected, whereas those of DMD with criterion are all about 0.5%.

Fig. 32 compares the error convergence at different initial conditions of the transient buffet flow case. In Fig. 32(a), different convergence trends are shown, especially when the number of selected DMD modes are less than 20. When seven modes are chosen, the largest error is about 10%, whereas the lowest error

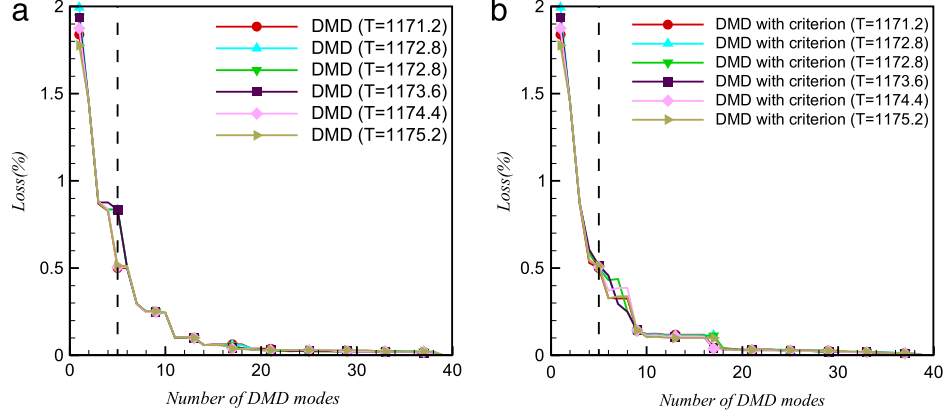


Fig. 31. Convergence of loss functions at different initial conditions of flow past a cylinder at the transient state. (a) DMD. (b) DMD with criterion.

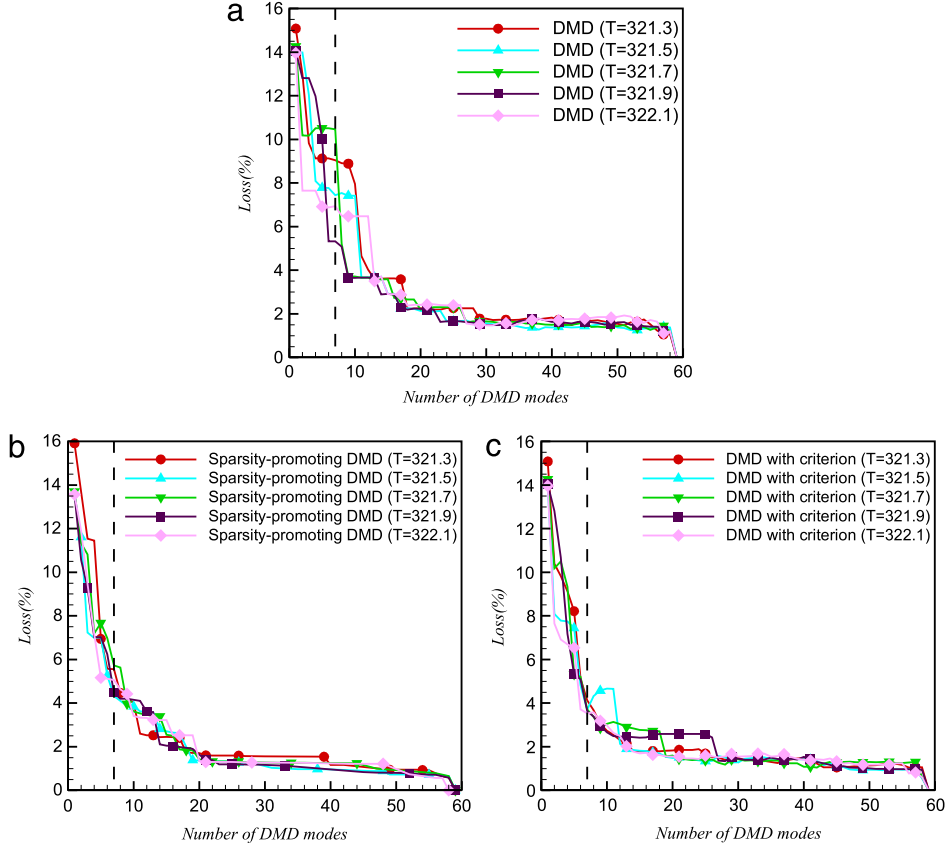


Fig. 32. Convergence of loss functions at different initial conditions of the buffet flow case at the transient state. (a) DMD. (b) Sparsity-promoting DMD. (c) DMD with criterion.

is larger than 5%. This phenomenon is unfavorable because if the residual error decreases in different manners, the user must try different initial conditions in order to get the best dynamic description. The cause of this problem is that when the flow is nonlinear, there are some modes have similar contribution to the initial condition, therefore correct modes with accurate stability characteristics are hard to identify from their amplitudes calculated in (25). Besides, some suboptimal but important modes may present less contribution to some initial conditions than numerically transient modes, so they cannot be the prior choice of DMD. In Fig. 32(b), the sensitivity to initial condition of sparsity-promoting DMD is also analyzed. Results indicate that due to the optimization of the amplitude vector, this approach gives the most smooth convergence on mode number, which has improved the performance of standard DMD approach. However,

due to the existence of transient modes with large decay-rate, the accuracy is not as low as using DMD with criterion approach. As shown in Fig. 32(c), for DMD with criterion approach, although small distinctions exist in the smoothness of convergence, the loss functions all come to 4% when seven modes are selected. The comparison indicates that using the proposed criterion, the influence of initial condition can be decreased, making DMD a more practical approach for some applications on modeling transient flow dynamics. Furthermore, even though the amplitude and eigenvalue are not corrected, this criterion will lead to a better accuracy with the same number of modes as the sparsity-promoting DMD approach, since it eliminates the influence of the large decay-rate transient modes. This indicates that an important precondition for obtaining good performance from sparsity-promoting or parametrized DMD approach [21] is that

the identified sparsity structure includes all the dominant dynamic modes, and the proposed criterion is capable of handling this task. However, it should also be noted that in Fig. 32(c), when using more than seven modes, the error for DMD with criterion even increases, which shows a higher dependency on the initial conditions than sparsity-promoting DMD. This problem occurs because the proposed criterion depends on the robustness of standard DMD in obtaining accurate description of DMD modes and eigenvalues, and it does not correct the amplitudes like sparsity-promoting DMD. Finally, it is worth mentioning that using DMD modes to predict the nonlinear systems is still a challenge and even more effective ROMs are needed in future works.

5. Conclusions

Although dynamic mode decomposition has been a useful tool for extracting coherent flow structures and analyzing complex flow phenomena, the selection of dominant DMD modes is not unique and most of current approaches are not effective and direct enough. In this paper, a criterion to select dominant DMD modes is introduced in order to obtain a more reasonable order of each mode's contribution to the whole dataset and construct better flow ROMs. The dominant modes are ranked according to their influence on the entire sampling space. This criterion gives different DMD approaches a generalized description and ranks dominant modes by temporal evolution of their time coefficients. The introduced DMD with criterion approach is applied to analyze and reconstruct both linear and nonlinear flow fields. Linear dynamics of a cylinder flow at $Re = 60$ are analyzed first, and a second-order frequency unstable mode ignored by standard DMD is captured by the proposed approach. Flow reconstruction indicates that this criterion outperforms the amplitude criterion taken from standard DMD approach in modeling linear flows. The transient state between linear equilibrium and limit cycle of the same cylinder flow is adopted as the second case where the flow with vortex shedding is correctly described. The last case is another transient state of a NACA0012 airfoil buffeting in transonic flow. The strong nonlinear characteristics caused by the interaction between the shock wave and the boundary layer are better captured by DMD with criterion than standard or the sparsity-promoting one. These cases illustrate that this criterion is well suited for unstable or transient flow states. All results indicate that this criterion helps to identify the dominant DMD modes of complex flows. Investigations on convergence show that the proposed criterion accelerates the decreasing of overall error as the selected number of DMD modes increases. And a favorable feature of this criterion is that the performance on flow reconstruction and prediction will not be readily disturbed by initial conditions, which makes this criterion outperforming standard DMD approach. Besides, because some transient DMD modes are eliminated, DMD equipped with the proposed criterion is capable of producing more accurate flow reconstruction with a smaller number of modes than sparsity-promoting DMD approach.

Acknowledgments

This work was supported by the National Natural Science Foundation of China (No. 11572252), the National Science Fund for Excellent Young Scholars (No. 11622220), Program for New Century Excellent Talents in University (No. NCET-13-0478), “111” project of China (No. B17037) and the Seed Foundation of Innovation and Creation for Graduate Students in Northwestern Polytechnical University (No. Z2016002). We fully appreciate the valuable comments from our reviewers.

References

- [1] W. Zhang, X. Li, Z. Ye, Y. Jiang, Mechanism of frequency lock-in in vortex-induced vibrations at low Reynolds numbers, *J. Fluid. Mech.* 783 (2015) 72–102. <http://dx.doi.org/10.1017/jfm.2015.548>.
- [2] J. Kou, W. Zhang, An approach to enhance the generalization capability of nonlinear aerodynamic reduced-order models, *Aerosp. Sci. Technol.* 49 (2016) 197–208. <http://dx.doi.org/10.1016/j.ast.2015.12.006>.
- [3] J. Kou, W. Zhang, M. Yin, Novel Wiener models with a time-delayed nonlinear block and their identification, *Nonlinear Dynam.* 85 (2016) 2389–2404. <http://dx.doi.org/10.1007/s11071-016-2833-y>.
- [4] W. Zhang, J. Kou, Z. Wang, Nonlinear aerodynamic reduced-order model for limit-cycle oscillation and flutter, *AIAA J.* 54 (2016) 3304–3311. <http://dx.doi.org/10.2514/1.j054951>.
- [5] B.R. Noack, K. Afanasiev, M. Morzyński, G. Tadmor, F. Thiele, A hierarchy of low-dimensional models for the transient and post-transient cylinder wake, *J. Fluid. Mech.* 497 (2003) 335–363. <http://dx.doi.org/10.1017/s0022112003006694>.
- [6] C.W. Rowley, Model reduction for fluids, using balanced proper orthogonal decomposition, *Int. J. Bifurcation Chaos* 15 (2005) 997–1013. <http://dx.doi.org/10.1142/s0218127405012429>.
- [7] C.W. Rowley, I. Mezić, S. Bagheri, P. Schlatter, D.S. Henningson, Spectral analysis of nonlinear flows, *J. Fluid. Mech.* 641 (2009) 115. <http://dx.doi.org/10.1017/s0022112009992059>.
- [8] P.J. Schmid, Dynamic mode decomposition of numerical and experimental data, *J. Fluid. Mech.* 656 (2010) 5–28. <http://dx.doi.org/10.1017/s0022112010001217>.
- [9] A. Barbagallo, D. Sipp, P.J. Schmid, Closed-loop control of an open cavity flow using reduced-order models, *J. Fluid. Mech.* 641 (2009) 1. <http://dx.doi.org/10.1017/s0022112009991418>.
- [10] A. Barbagallo, D. Sipp, P.J. Schmid, Input-output measures for model reduction and closed-loop control: application to global modes, *J. Fluid. Mech.* 685 (2011) 23–53. <http://dx.doi.org/10.1017/jfm.2011.271>.
- [11] M. Fossati, Evaluation of aerodynamic loads via reduced-order methodology, *AIAA J.* 53 (2015) 2389–2405. <http://dx.doi.org/10.2514/1.j053755>.
- [12] D. Xiao, P. Yang, F. Fang, J. Xiang, C.C. Pain, I.M. Navon, Non-intrusive reduced order modelling of fluid-structure interactions, *Comput. Methods Appl. Mech. Engrg.* 303 (2016) 35–54. <http://dx.doi.org/10.1016/j.cma.2015.12.029>.
- [13] X. Ma, G.E. Karniadakis, A low-dimensional model for simulating three-dimensional cylinder flow, *J. Fluid. Mech.* 458 (2002) <http://dx.doi.org/10.1017/s0022112002007991>.
- [14] R.m. Bourguet, M. Braza, A. Dervieux, Reduced-order modeling for unsteady transonic flows around an airfoil, *Phys. Fluids* 19 (2007) 111701. <http://dx.doi.org/10.1063/1.2800042>.
- [15] S. Walton, O. Hassan, K. Morgan, Reduced order modelling for unsteady fluid flow using proper orthogonal decomposition and radial basis functions, *Appl. Math. Model.* 37 (2013) 8930–8945. <http://dx.doi.org/10.1016/j.apm.2013.04.025>.
- [16] A. Seena, H.J. Sung, Dynamical mode decomposition of turbulent cavity flows for self-sustained oscillations, *Int. J. Heat Fluid Flow* 32 (2011) 1098–1110. <http://dx.doi.org/10.1016/j.ijheatfluidflow.2011.09.008>.
- [17] D. Duke, J. Soria, D. Honnery, An error analysis of the dynamic mode decomposition, *Exp. Fluids* 52 (2012) 529–542. <http://dx.doi.org/10.1007/s00348-011-1235-7>.
- [18] T.W. Muld, G. Efraimsson, D.S. Henningson, Flow structures around a high-speed train extracted using proper orthogonal decomposition and dynamic mode decomposition, *Comput. Fluids* 57 (2012) 87–97. <http://dx.doi.org/10.1016/j.compfluid.2011.12.012>.
- [19] S. Sarmast, R. Dadfar, R.F. Mikkelsen, P. Schlatter, S. Ivanell, J.N. Sørensen, D.S. Henningson, Mutual inductance instability of the tip vortices behind a wind turbine, *J. Fluid. Mech.* 755 (2014) 705–731. <http://dx.doi.org/10.1017/jfm.2014.326>.
- [20] M.R. Jovanović, P.J. Schmid, J.W. Nichols, Sparsity-promoting dynamic mode decomposition, *Phys. Fluids* 26 (2014) 024103. <http://dx.doi.org/10.1063/1.4863670>.
- [21] T. Sayadi, P.J. Schmid, F. Richecoeur, D. Durox, Parametrized data-driven decomposition for bifurcation analysis, with application to thermo-acoustically unstable systems, *Phys. Fluids* 27 (2015) 037102. <http://dx.doi.org/10.1063/1.4913868>.
- [22] K.K. Chen, J.H. Tu, C.W. Rowley, Variants of dynamic mode decomposition: boundary condition, Koopman, and Fourier analyses, *J. Nonlinear Sci.* 22 (2012) 887–915. <http://dx.doi.org/10.1007/s00332-012-9130-9>.
- [23] A. Wynn, D.S. Pearson, B. Ganapathisubramani, P.J. Goulart, Optimal mode decomposition for unsteady flows, *J. Fluid. Mech.* 733 (2013) 473–503. <http://dx.doi.org/10.1017/jfm.2013.426>.
- [24] S.T.M. Dawson, M.S. Hemati, M.O. Williams, C.W. Rowley, Characterizing and correcting for the effect of sensor noise in the dynamic mode decomposition, *Exp. Fluids* 57 (2016) <http://dx.doi.org/10.1007/s00348-016-2127-7>.
- [25] R. Leroux, L. Cordiner, Dynamic mode decomposition for non-uniformly sampled data, *Exp. Fluids* 57 (2016) <http://dx.doi.org/10.1007/s00348-016-2165-1>.
- [26] S.L. Brunton, J.L. Proctor, J.H. Tu, J.N. Kutz, Compressed sensing and dynamic mode decomposition, *J. Comput. Dyn.* 2 (2016) 165–191. <http://dx.doi.org/10.3934/jcd.2015002>.

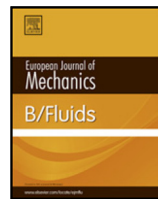
- [27] S.L. Brunton, J.H. Tu, I. Bright, J.N. Kutz, Compressive sensing and low-rank libraries for classification of bifurcation regimes in nonlinear dynamical systems, *SIAM J. Appl. Dyn. Syst.* 13 (2014) 1716–1732. <http://dx.doi.org/10.1137/130949282>.
- [28] J.N. Kutz, X. Fu, S.L. Brunton, Multiresolution dynamic mode decomposition, *SIAM J. Appl. Dyn. Syst.* 15 (2016) 713–735. <http://dx.doi.org/10.1137/15m1023543>.
- [29] S. Sargsyan, S.L. Brunton, J.N. Kutz, Nonlinear model reduction for dynamical systems using sparse sensor locations from learned libraries, *Phys. Rev. E* 92 (2015) 033304. <http://dx.doi.org/10.1103/PhysRevE.92.033304>.
- [30] S. Bagheri, Effects of weak noise on oscillating flows: Linking quality factor, Floquet modes, and Koopman spectrum, *Phys. Fluids* 26 (2014) 094104. <http://dx.doi.org/10.1063/1.4895898>.
- [31] M.S. Hemati, M.O. Williams, C.W. Rowley, Dynamic mode decomposition for large and streaming datasets, *Phys. Fluids* 26 (2014) 111701. <http://dx.doi.org/10.1063/1.4901016>.
- [32] J.H. Tu, C.W. Rowley, J.N. Kutz, J.K. Shang, Spectral analysis of fluid flows using sub-Nyquist-rate PIV data, *Exp. Fluids* 55 (2014) 1805. <http://dx.doi.org/10.1007/s00348-014-1805-6>.
- [33] F. Guénat, L. Mathelin, L.R. Pastur, A dynamic mode decomposition approach for large and arbitrarily sampled systems, *Phys. Fluids* 27 (2015) 025113. <http://dx.doi.org/10.1063/1.4908073>.
- [34] J.L. Proctor, S.L. Brunton, J.N. Kutz, Dynamic mode decomposition with control, *SIAM J. Appl. Dyn. Syst.* 15 (2016) 142–161. <http://dx.doi.org/10.1137/15m1013857>.
- [35] J. Annoni, P. Seiler, A method to construct reduced-order parameter-varying models, *Int. J. Robust. Nonlinear Control* (2016). <http://dx.doi.org/10.1002/rnc.3586>.
- [36] B.R. Noack, Recursive dynamic mode decomposition of a cylinder wake, 2015. ArXiv e-prints <arXiv:1511.06876v06871>.
- [37] G. He, J. Wang, C. Pan, Initial growth of a disturbance in a boundary layer influenced by a circular cylinder wake, *J. Fluid. Mech.* 718 (2013) 116–130. <http://dx.doi.org/10.1017/jfm.2012.599>.
- [38] Z.-H. Wan, L. Zhou, B.-F. Wang, D.-J. Sun, Dynamic mode decomposition of forced spatially developed transitional jets, *Eur. J. Mech. B Fluids* 51 (2015) 16–26. <http://dx.doi.org/10.1016/j.euromechflu.2014.12.001>.
- [39] A. Ducouin, J.C. Loiseau, J.C. Robinet, Numerical investigation of the interaction between laminar to turbulent transition and the wake of an airfoil, *Eur. J. Mech. B Fluids* 57 (2016) 231–248. <http://dx.doi.org/10.1016/j.euromechflu.2016.01.005>.
- [40] V. Statnikov, I. Bolgar, S. Scharnowski, M. Meinke, C.J. Kähler, W. Schröder, Analysis of characteristic wake flow modes on a generic transonic backward-facing step configuration, *Eur. J. Mech. B Fluids* 59 (2016) 124–134. <http://dx.doi.org/10.1016/j.euromechflu.2016.05.008>.
- [41] C.W. Rowley, S.T.M. Dawson, Model reduction for flow analysis and control, *Annu. Rev. Fluid Mech.* 49 (2017) 387–417. <http://dx.doi.org/10.1146/annurev-fluid-010816-060042>.
- [42] P.J. Schmid, D. Violato, F. Scarano, Decomposition of time-resolved tomographic PIV, *Exp. Fluids* 52 (2012) 1567–1579. <http://dx.doi.org/10.1007/s00348-012-1266-8>.
- [43] T. Sayadi, Peter J. Schmid, J.W. Nichols, P. Moin, Reduced-order representation of near-wall structures in the late transitional boundary layer, *J. Fluid. Mech.* 748 (2014) 278–301. <http://dx.doi.org/10.1017/jfm.2014.184>.
- [44] J.H. Tu, C.W. Rowley, D.M. Luchtenburg, S.L. Brunton, J.N. Kutz, On dynamic mode decomposition: theory and applications, *J. Comput. Dyn.* 1 (2014) 391–421. <http://dx.doi.org/10.3934/jcd.2014.1.391>.
- [45] G. Tissot, L. Cordier, N. Benard, B.R. Noack, Model reduction using dynamic mode decomposition, *C. R. Mec.* 342 (2014) 410–416. <http://dx.doi.org/10.1016/j.crme.2013.12.011>.
- [46] I. Mezić, Analysis of fluid flows via spectral properties of the Koopman operator, *Annu. Rev. Fluid Mech.* 45 (2013) 357–378. <http://dx.doi.org/10.1146/annurev-fluid-011212-140652>.
- [47] S. Bagheri, Koopman-mode decomposition of the cylinder wake, *J. Fluid. Mech.* 726 (2013) 596–623. <http://dx.doi.org/10.1017/jfm.2013.249>.
- [48] D.L. Donoho, M. Gavish, The optimal hard threshold for singular values is $4/\sqrt{3}$, 2014. ArXiv e-prints.
- [49] P. Spalart, S. Allmaras, A one-equation turbulence model for aerodynamic flows, *AIAA Paper*, 1992, p. 0439.
- [50] C. Gao, W. Zhang, Y. Liu, Z. Ye, Y. Jiang, Numerical study on the correlation of transonic single-degree-of-freedom flutter and buffet, *Sci. China Phys. Mech.* 58 (2015) 084701. <http://dx.doi.org/10.1007/s11433-015-5683-6>.
- [51] W. Zhang, C. Gao, Y. Liu, Z. Ye, Y. Jiang, The interaction between flutter and buffet in transonic flow, *Nonlinear Dynam.* 82 (2015) 1851–1865. <http://dx.doi.org/10.1007/s11071-015-2282-z>.
- [52] Y. Jiang, (Ph.D. dissertation), Northwestern Polytechnical University, Xi'an, China, 2013.
- [53] Q. Zhang, Y. Liu, S. Wang, The identification of coherent structures using proper orthogonal decomposition and dynamic mode decomposition, *J. Fluid. Struct.* 49 (2014) 53–72. <http://dx.doi.org/10.1016/j.jfluidstructs.2014.04.002>.
- [54] J. Kou, W. Zhang, C. Gao, Modal analysis of transonic buffet based on POD and DMD techniques, *Acta Aeronaut. Astronaut. Sin.* 37 (2016) 2679–2689. <http://dx.doi.org/10.7527/S1000-6893.2016.0003>.
- [55] C. Gao, W. Zhang, Z. Ye, Numerical study on closed-loop control of transonic buffet suppression by trailing edge flap, *Comput. Fluids* 132 (2016) 32–45. <http://dx.doi.org/10.1016/j.compfluid.2016.03.031>.

Update

European Journal of Mechanics / B Fluids

Volume 68, Issue , March - April 2018, Page 219

DOI: <https://doi.org/10.1016/j.euromechflu.2017.12.003>



Corrigendum to “An improved criterion to select dominant modes from dynamic mode decomposition” [Eur. J. Mech. B Fluids 62 (2017) 109–129]

Jiaqing Kou, Weiwei Zhang*

School of Aeronautics, Northwestern Polytechnical University, Xi'an 710072, China



ARTICLE INFO

Article history:

Available online 21 December 2017

The authors regret that Eqs. (11), (27), (35) include some minor errors. Eqs. (11) and (27), which describe the process of flow reconstruction, should be changed as follows:

$$\begin{aligned} \mathbf{X} &= [\mathbf{x}_1, \dots, \mathbf{x}_{N-1}] = \mathbf{DT} \\ &= [\mathbf{d}_1, \dots, \mathbf{d}_m] \begin{bmatrix} 1 & \lambda_1 & \dots & \lambda_1^{N-2} \\ 1 & \lambda_2 & \dots & \lambda_2^{N-2} \\ \vdots & \ddots & \ddots & \ddots \\ 1 & \lambda_m & \dots & \lambda_m^{N-2} \end{bmatrix} \quad (11) \end{aligned}$$

$$\mathbf{X} = [\mathbf{x}_1, \mathbf{x}_2, \mathbf{x}_3, \dots, \mathbf{x}_{N-1}] = \Phi \mathbf{D}_\alpha \mathbf{V}_{and}$$

$$= [\Phi_1, \Phi_2, \dots, \Phi_r] \begin{bmatrix} \alpha_1 & & & \\ & \alpha_2 & & \\ & & \ddots & \\ & & & \alpha_r \end{bmatrix} \times \begin{bmatrix} 1 & \mu_1 & \dots & (\mu_1)^{N-2} \\ 1 & \mu_2 & \dots & (\mu_2)^{N-2} \\ \vdots & \ddots & \ddots & \ddots \\ 1 & \mu_r & \dots & (\mu_r)^{N-2} \end{bmatrix} \quad (27)$$

Moreover, we want to point out that, the value in Eq. (35) should be defined as the root mean squared error (*rmse*), rather than the mean squared error (*mse*) in the original manuscript. The authors would like to apologise for any inconvenience caused.

DOI of original article: <http://dx.doi.org/10.1016/j.euromechflu.2016.11.015>.

* Corresponding author.

E-mail addresses: koujiaqing93@163.com (J. Kou), [\(W. Zhang\).](mailto:aeroelastic@nwpu.edu.cn)